








Exploring SMEFT couplings using the forward–backward asymmetry in neutral current Drell–Yan production at the LHC

Andrii Anataichuk^{1,2,a}, Sven-Olaf Moch^{3,b}, and the xFitter Developers' team: Hamed Abdolmaleki^{4,5,c} , Simone Amoroso^{6,d}, Daniel Britzger^{7,e}, Filippo Dattola^{6,f}, Juri Fiaschi^{8,g} , Francesco Giuli^{9,h} , Alexander Glazov^{6,i}, Francesco Hautmann^{9,10,11,j}, Agnieszka Luszczak^{12,k}, Sara Taheri Monfared^{6,l} , Fred Olness^{13,m}, Federico Vazzoler^{6,n}, Oleksandr Zenaiev^{3,o} 

¹ V. N. Karazin Kharkiv National University, Kharkiv, Ukraine

² Taras Shevchenko National University of Kyiv, Kyiv, Ukraine

³ Hamburg University, Hamburg, Germany

⁴ School of Physics, Institute for Research in Fundamental Sciences (IPM), Tehran, Iran

⁵ Department of Physics, Faculty of Science, Malayer University, Malayer, Iran

⁶ Deutsches Elektronen-Synchrotron DESY, Hamburg, Germany

⁷ Max Planck Institute, Munich, Germany

⁸ Università degli Studi di Milano-Bicocca and INFN, Milan, Italy

⁹ CERN, Geneva, Switzerland

¹⁰ University of Antwerp, Antwerpen, Belgium

¹¹ University of Oxford, Oxford, UK

¹² Cracow University of Technology, Cracow, Poland

¹³ SMU Physics, Dallas, USA

Received: 16 August 2024 / Accepted: 9 October 2024
© The Author(s) 2024

Abstract Neutral current Drell–Yan (DY) lepton-pair production is considered to study Z -boson quark couplings. Using the open-source fit platform `xFitter`, we investigate the impact of high-statistics measurements of the neutral current DY (NCDY) forward–backward asymmetry A_{FB} near the weak boson mass scale in the present and forth-

coming stages of the Large Hadron Collider (LHC). Besides recovering earlier results on the A_{FB} sensitivity to parton distribution functions, we analyze the precision determination of Z -boson couplings to left-handed and right-handed u -quarks and d -quarks, and explore Beyond-Standard-Model contributions using the Standard Model Effective Field Theory (SMEFT) framework. We perform a sensitivity study and comment on the role of the A_{FB} asymmetry for the electroweak SMEFT fit and precision Z -boson physics at the LHC and high-luminosity HL-LHC.

A. Anataichuk: on leave.

^a e-mail: andanataychuk@gmail.com

^b e-mail: sven-olaf.moch@desy.de

^c e-mail: Hamed.Abdolmaleki@desy.de

^d e-mail: simone.amoroso@desy.de

^e e-mail: britzger@mpp.mpg.de

^f e-mail: filippo.dattola@desy.de

^g e-mail: Juri.Fiaschi@liverpool.ac.uk

^h e-mail: francesco.giuli@cern.ch

ⁱ e-mail: alexander.glazov@desy.de

^j e-mail: hautmann@thphys.ox.ac.uk

^k e-mail: agnieszka.luszczak@desy.de

^l e-mail: taheri@mail.desy.de

^m e-mail: olness@smu.edu

ⁿ e-mail: federico.vazzoler@cern.ch

^o e-mail: oleksandr.zenaiev@desy.de (corresponding author)

1 Introduction

The physics program centering on electroweak (EW) precision observables receives essential inputs from measurements of W and Z bosons at the LHC. Owing to the cancellation of many systematic uncertainties, the forward–backward asymmetry A_{FB} in NCDY lepton-pair production is a crucial component of this program. The A_{FB} asymmetry is employed for determinations of the weak mixing angle θ_W from LHC measurements at the Z -pole [1–4], complementing LEP/SLD [5] and Tevatron [6] results.

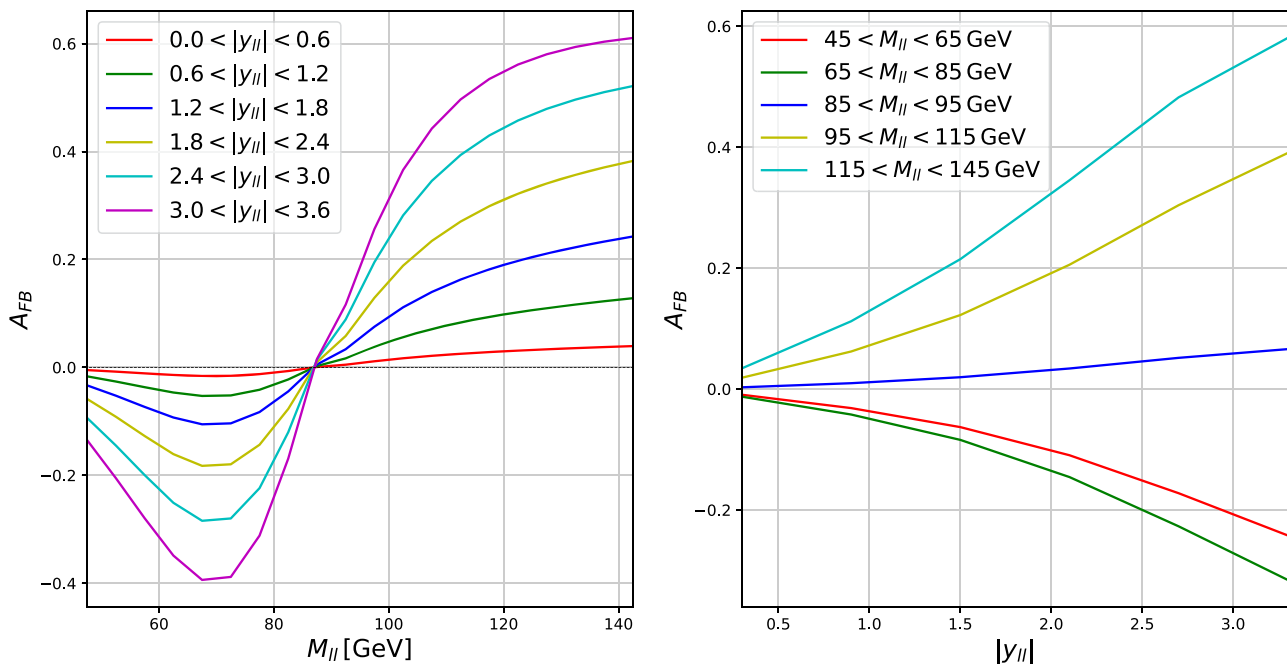


Fig. 1 The predicted A_{FB} as a function of the invariant mass of the dilepton system in different rapidity intervals (left) and rapidity of the dilepton system in different invariant mass intervals (right) at LO in the SM

Given that parton distribution functions (PDFs) constitute one of the dominant uncertainty sources in the precision EW physics program at the LHC, it is especially relevant that the A_{FB} asymmetry has been shown to provide us with new sensitivity to PDFs [7–11]. This sensitivity is currently not exploited in global PDF extractions [12–16], and could potentially lead to dramatic improvements in our knowledge of PDFs. This applies, in particular, in kinematic regions which are relevant for new physics searches in the multi-TeV region at the LHC, for instance in the context of Beyond-Standard-Model (BSM) heavy Z' [17, 18] and W' bosons [19], and photon-induced di-lepton production processes [20–22].

Furthermore, as in Ref. [11] the impact of the forward-backward A_{FB} asymmetry in the neutral current sector may be combined with that of the lepton-charge A_W asymmetry in the charged current sector. This points to strategies which are alternative to those taken in experimental analyses such as in Refs. [1, 3, 23], and aim at exploiting new measurements, capable of providing sensitivity to PDFs with low theoretical and experimental systematics while controlling correlations. Related investigations of the A_{FB} asymmetry in Ref. [24] focus on the behaviour induced by the NNPDF4.0 set [14]. See also the studies [25–30] based on the package EPUMP [31, 32].

To systematically investigate the role of the asymmetry in precision EW measurements, searches for BSM phenomena, and determinations of PDFs, a well-established framework

is provided by the Standard Model Effective Field Theory (SMEFT) [33]. Details can be found in recent reviews [34, 35] and SMEFT fitting packages [36–38]. Recent SMEFT studies of precision electroweak observables in di-lepton channels at the LHC have been performed in Refs. [39–44] and analogous studies on the role of PDFs in BSM searches in Refs. [45, 46].

In this paper we will concentrate on A_{FB} asymmetry measurements in NCDY production in the region near the Z -boson mass scale. The analysis will be performed in the framework of the SMEFT Lagrangian, including operators up to dimension $D = 6$ [33, 47],

$$\mathcal{L} = \mathcal{L}^{(\text{SM})} + \frac{1}{\Lambda^2} \sum_{j=1}^{N_6} C_j^{(6)} \mathcal{O}_j^{(6)}, \quad (1)$$

where the first term on the right hand side is the SM Lagrangian, consisting of operators of mass dimension $D = 4$, while the next term is the EFT contribution containing N_6 operators \mathcal{O}_j of mass dimension $D = 6$, each weighted by the dimensionless Wilson coefficient C_j divided by Λ^2 , where Λ is the ultraviolet mass scale of the EFT.

In the di-lepton mass region near the Z -boson peak, four-fermion operators and dipole operators coupling fermions and vector bosons can be neglected [39, 43] in Eq. (1), and the whole effect of the $D = 6$ SMEFT Lagrangian is a modification of the vector boson couplings to fermions. Using LEP constraints [5], corrections to Z -boson couplings to leptons

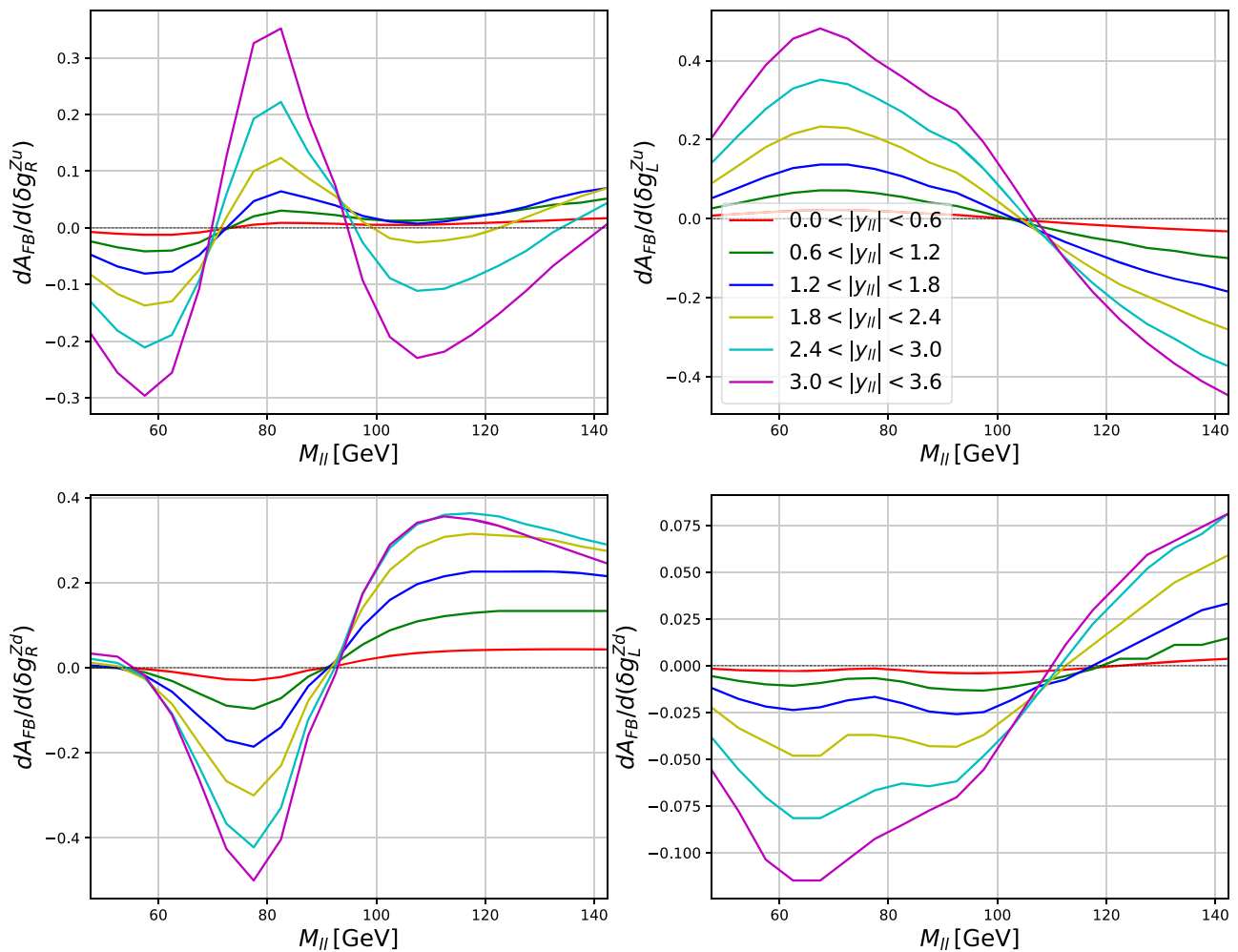


Fig. 2 The partial derivatives of the predicted A_{FB} with respect to δg_R^{Zu} (upper left), δg_L^{Zu} (upper right), δg_R^{Zd} (lower left) and δg_L^{Zd} (lower right) couplings as a function of the invariant mass of the dilepton system in different rapidity intervals at LO

can also be neglected [43]. We will thus focus on the SMEFT corrections to Z -boson couplings to u -type (including c) and d -type (including s, b) quarks, that are least constrained by LEP and have not comprehensively been studied at the LHC.

To explore these SMEFT couplings, we will extend the implementation of the A_{FB} asymmetry provided in Ref. [9], using the quantum chromodynamics (QCD) fit platform `xFitter` (formerly known as `HERAFitter`) [48–50]. As a check, we will recover the results of Ref. [9] on PDF extracted from A_{FB} pseudodata, and in addition we will obtain new constraints on Z -boson vector and axial couplings. We will examine the projected luminosity scenario of 3000 fb^{-1} for the High-Luminosity LHC (HL-LHC) [51–53].

The paper is organized as follows. In Sect. 2 we present the SMEFT treatment of the NCDY di-lepton production process in terms of EFT corrections to the SM couplings, and its implementation to make predictions for the A_{FB} asymmetry in `xFitter`. In Sect. 3 we describe the A_{FB} pseudodata

generation. In Sect. 4 we carry out the main analysis within `xFitter`, leading to the determination of the SMEFT couplings. In Sect. 5 we give conclusions.

2 A_{FB} within SMEFT in `xFitter`

In this section we start by describing the $D = 6$ SMEFT Lagrangian for Z -boson interactions with fermions, and introduce the SMEFT couplings for left-handed and right-handed u -quarks and d -quarks. Next we define the SMEFT vector and axial couplings, and express the forward–backward asymmetry A_{FB} in terms of these couplings. We discuss the extension of the `xFitter` implementation [9] for A_{FB} to the SMEFT case.

The SMEFT Lagrangian for the coupling of the Z -boson to fermions is given by

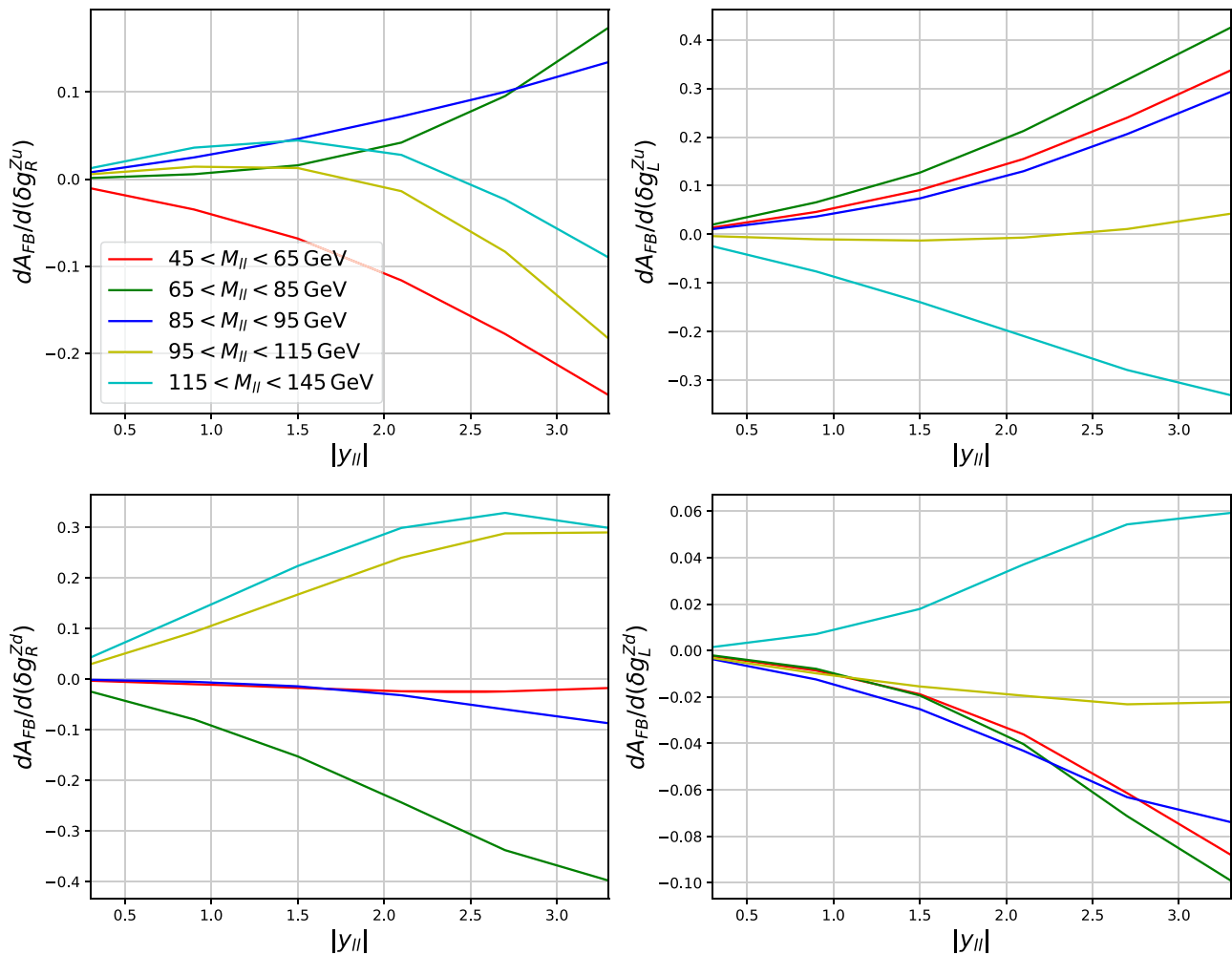


Fig. 3 The partial derivatives of the predicted A_{FB} with respect to δg_R^{Zu} (upper left), δg_L^{Zu} (upper right), δg_R^{Zd} (lower left) and δg_L^{Zd} (lower right) couplings as a function of the rapidity of the dilepton system in different invariant mass intervals at LO

$$\begin{aligned}
 \mathcal{L}_Z^{(\text{SMEFT})} = & 2M_Z \sqrt{G_\mu} \sqrt{2} Z^\alpha \left\{ \bar{q}_L \gamma_\alpha \left(g_{L(\text{SM})}^{Zq} \right. \right. \\
 & + \delta g_L^{Zq} \Big) q_L + \bar{u}_R \gamma_\alpha \left(g_{R(\text{SM})}^{Zu} + \delta g_R^{Zu} \right) u_R \\
 & + \bar{d}_R \gamma_\alpha \left(g_{R(\text{SM})}^{Zd} + \delta g_R^{Zd} \right) d_R \\
 & + \{\text{leptonic terms}\} \Big\}. \tag{2}
 \end{aligned}$$

Here q_L is the left-handed quark SU(2) doublet, while u_R and d_R are the right-handed quark SU(2) singlets. The left-handed and right-handed quark SM couplings are expressed in terms of the weak mixing angle θ_W as follows,

$$\begin{aligned}
 g_{R(\text{SM})}^{Zu} &= 1/2 - 2/3 \sin^2 \theta_W, \\
 g_{L(\text{SM})}^{Zu} &= -2/3 \sin^2 \theta_W, \\
 g_{R(\text{SM})}^{Zd} &= -1/2 + 1/3 \sin^2 \theta_W, \\
 g_{L(\text{SM})}^{Zd} &= 1/3 \sin^2 \theta_W. \tag{3}
 \end{aligned}$$

The SMEFT couplings are obtained from the SM couplings via the corrections δg , i.e., $g(\text{SMEFT}) \equiv g(\text{SM}) + \delta g$:

$$\begin{aligned}
 g_L^{Zu} &\equiv g_{L(\text{SMEFT})}^{Zu} = g_{L(\text{SM})}^{Zu} + \delta g_L^{Zu}, \\
 g_R^{Zu} &\equiv g_{R(\text{SMEFT})}^{Zu} = g_{R(\text{SM})}^{Zu} + \delta g_R^{Zu}, \\
 g_L^{Zd} &\equiv g_{L(\text{SMEFT})}^{Zd} = g_{L(\text{SM})}^{Zd} + \delta g_L^{Zd}, \\
 g_R^{Zd} &\equiv g_{R(\text{SMEFT})}^{Zd} = g_{R(\text{SM})}^{Zd} + \delta g_R^{Zd}. \tag{4}
 \end{aligned}$$

In our analysis, we assume $\delta g_{R,L}^{Zd} = \delta g_{R,L}^{Zs} = \delta g_{R,L}^{Zb}$ and $\delta g_{R,L}^{Zu} = \delta g_{R,L}^{Zc}$. The contributions from heavy c - and b -quarks are small, of the order of 10%. The vector and axial couplings of the Z -boson are defined by taking the combinations $L \pm R$ of the left-handed and right-handed fermion couplings. So the SMEFT vector and axial couplings are given by

$$\begin{aligned}
 g_V^{Zu} &= g_R^{Zu} + g_L^{Zu}, & g_A^{Zu} &= g_R^{Zu} - g_L^{Zu}, \\
 g_V^{Zd} &= g_R^{Zd} + g_L^{Zd}, & g_A^{Zd} &= g_R^{Zd} - g_L^{Zd}. \tag{5}
 \end{aligned}$$

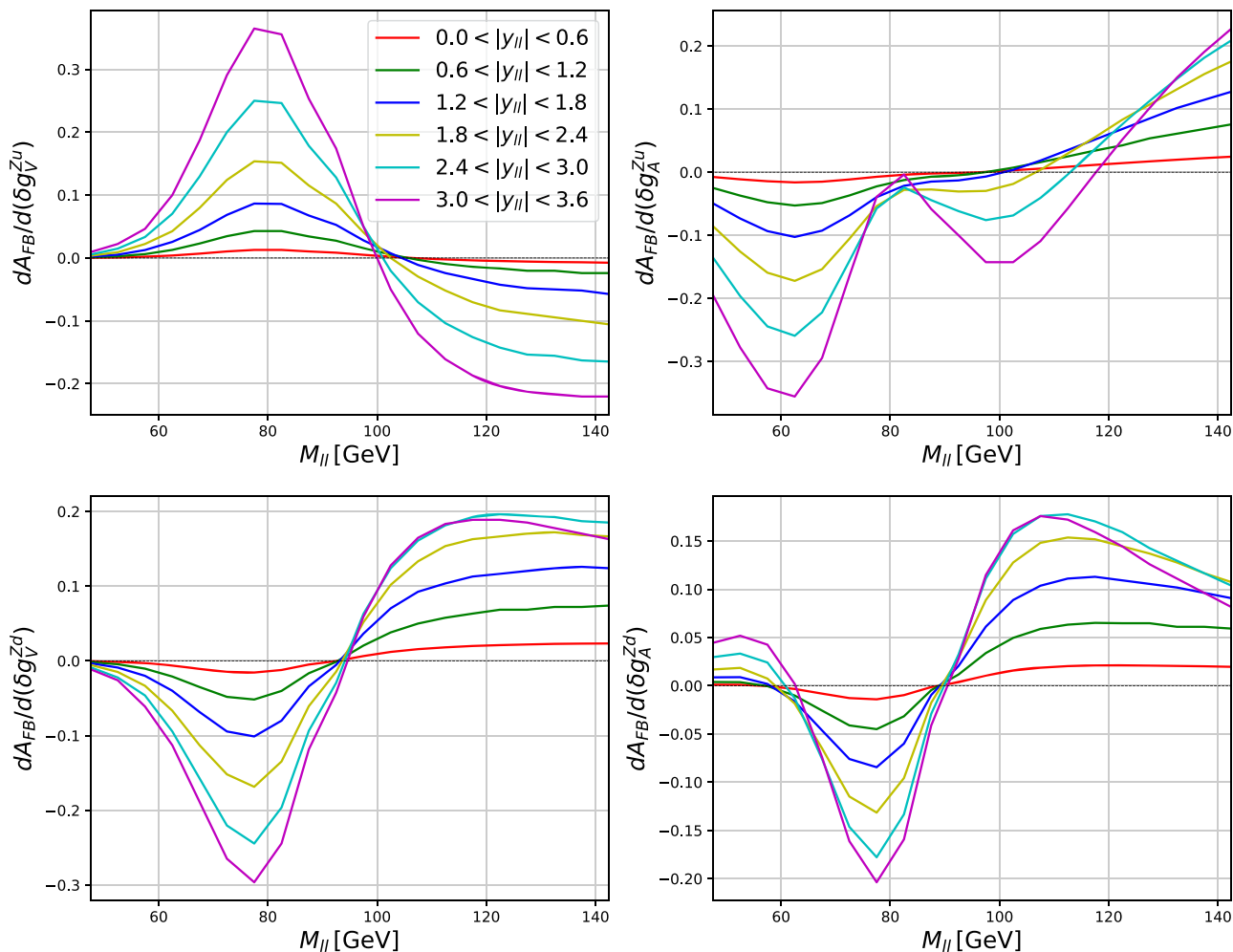


Fig. 4 Same as in Fig. 2 for the axial and vector couplings

In order to maximize the sensitivity, we consider the DY triple-differential cross section in the di-lepton invariant mass $M_{\ell\ell}$, di-lepton rapidity $y_{\ell\ell}$ and angular variable θ^* between the outgoing lepton and the incoming quark in the Collins–Soper (CS) reference frame [54]. In this frame, the decay angle is measured from an axis symmetric with respect to the two incoming partons. The expression for the angle θ^* in the CS frame is given by

$$\cos \theta^* = \frac{p_{Z,\ell\ell}}{M_{\ell\ell}|p_{Z,\ell\ell}|} \frac{p_1^+ p_2^- - p_1^- p_2^+}{\sqrt{M_{\ell\ell}^2 + p_{T,\ell\ell}^2}}, \tag{6}$$

where $p_i^\pm = E_i \pm p_{z,i}$ and the index $i = 1, 2$ corresponds to the positive and negative charged lepton respectively. Here E and p_z are the energy and the z -components of the leptonic four-momentum, respectively; $p_{Z,\ell\ell}$ is the di-lepton z -component of the momentum and $p_{T,\ell\ell}$ is the di-lepton transverse momentum. At leading order (LO) in QCD and

EW theory, this cross section can be written as

$$\frac{d^3\sigma}{dM_{\ell\ell} dy_{\ell\ell} d\cos\theta^*} = \frac{\pi\alpha^2}{3M_{\ell\ell}s} \sum_q P_q \left[f_q(x_1, Q^2) \times f_{\bar{q}}(x_2, Q^2) + f_{\bar{q}}(x_1, Q^2) \times f_q(x_2, Q^2) \right], \tag{7}$$

where s is the square of the centre-of-mass energy of the collision, $x_{1,2} = M_{\ell\ell} e^{\pm y_{\ell\ell}} / \sqrt{s}$ are the momentum fractions of the initial-state partons, $f_{q,\bar{q}}(x_i, Q^2)$ are their PDFs, Q^2 is the squared factorization scale, and the factor P_q contains the propagators and couplings of the Z -boson, photon, and Z - γ interference,

$$P_q = e_\ell^2 e_q^2 (1 + \cos^2 \theta^*) + \frac{M_{\ell\ell}^2 (M_{\ell\ell}^2 - M_Z^2)}{2 \sin^2 \theta_W \cos^2 \theta_W [(M_{\ell\ell}^2 - M_Z^2)^2 + \Gamma_Z^2 M_Z^2]} \times (e_\ell e_q) \left[g_V^{Z\ell} g_V^{Zq} (1 + \cos^2 \theta^*) + 2g_A^{Z\ell} g_A^{Zq} \cos \theta^* \right]$$

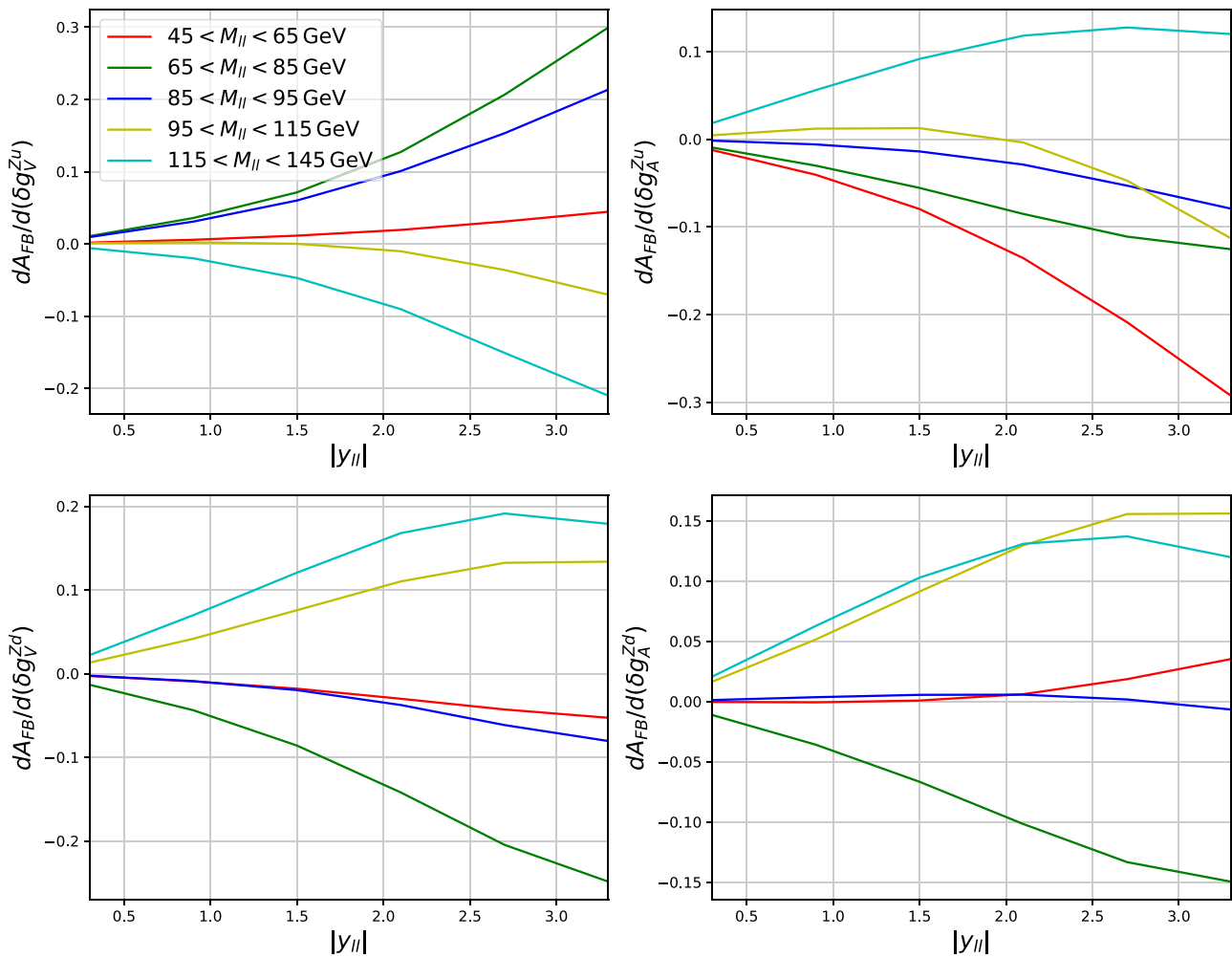


Fig. 5 Same as in Fig. 3 for the axial and vector couplings

$$\begin{aligned}
 & + \frac{M_{\ell\ell}^4}{16 \sin^4 \theta_W \cos^4 \theta_W [(M_{\ell\ell}^2 - M_Z^2)^2 + \Gamma_Z^2 M_Z^2]} \\
 & \times \left\{ [(g_A^{Z\ell})^2 + (g_V^{Z\ell})^2][(g_A^{Zq})^2 + (g_V^{Zq})^2] \right. \\
 & \left. \times (1 + \cos^2 \theta^*) + 8g_A^{Z\ell} g_V^{Z\ell} g_A^{Zq} g_V^{Zq} \cos \theta^* \right\}. \quad (8)
 \end{aligned}$$

Here M_Z and Γ_Z are the mass and the width of the Z boson, e_ℓ and e_q are the lepton and quark electric charges, $g_V^{Z\ell} = -1/2 + 2 \sin^2 \theta_W$ and $g_A^{Z\ell} = -1/2$ are the vector and axial couplings of leptons, and g_V^{Zq} and g_A^{Zq} are the SMEFT vector and axial couplings of quarks in Eqs. (4), (5). The first and third terms on the right hand side of Eq. (8) are the square of the s -channel diagrams with photon and Z -boson mediators respectively, while the second term is the interference between the two.

The forward–backward asymmetry A_{FB}^* is defined as

$$A_{\text{FB}}^* = \left(d^2\sigma/dM_{\ell\ell} dy_{\ell\ell} [\cos \theta^* > 0] \right.$$

$$\begin{aligned}
 & \left. - d^2\sigma/dM_{\ell\ell} dy_{\ell\ell} [\cos \theta^* < 0] \right) \\
 & / \left(d^2\sigma/dM_{\ell\ell} dy_{\ell\ell} [\cos \theta^* > 0] \right. \\
 & \left. + d^2\sigma/dM_{\ell\ell} dy_{\ell\ell} [\cos \theta^* < 0] \right). \quad (9)
 \end{aligned}$$

We will consider the measurement of the A_{FB}^* asymmetry differentially in $M_{\ell\ell}$ and $y_{\ell\ell}$ according to Eqs. (7), (9).

To perform this study, we extend the implementation [9] of the A_{FB}^* asymmetry in the `xFitter` platform [48, 49] to (i) include the SMEFT couplings described above in Eqs. (4), (5), and (ii) upgrade the calculations to double-differential distributions in both invariant mass $M_{\ell\ell}$ and rapidity $y_{\ell\ell}$ of the di-lepton final-state system. The collider energy, acceptance cuts and bin boundaries in $M_{\ell\ell}$ and $y_{\ell\ell}$ are adjustable parameters in the present computation. Fiducial selections are applied to the leptons, by requiring them to have a transverse momentum $p_T^\ell > 20$ GeV and pseudorapidity $|\eta_\ell| < 5$. The mass effects of charm and bottom quarks in the matrix element are neglected, as appropriate for a high-

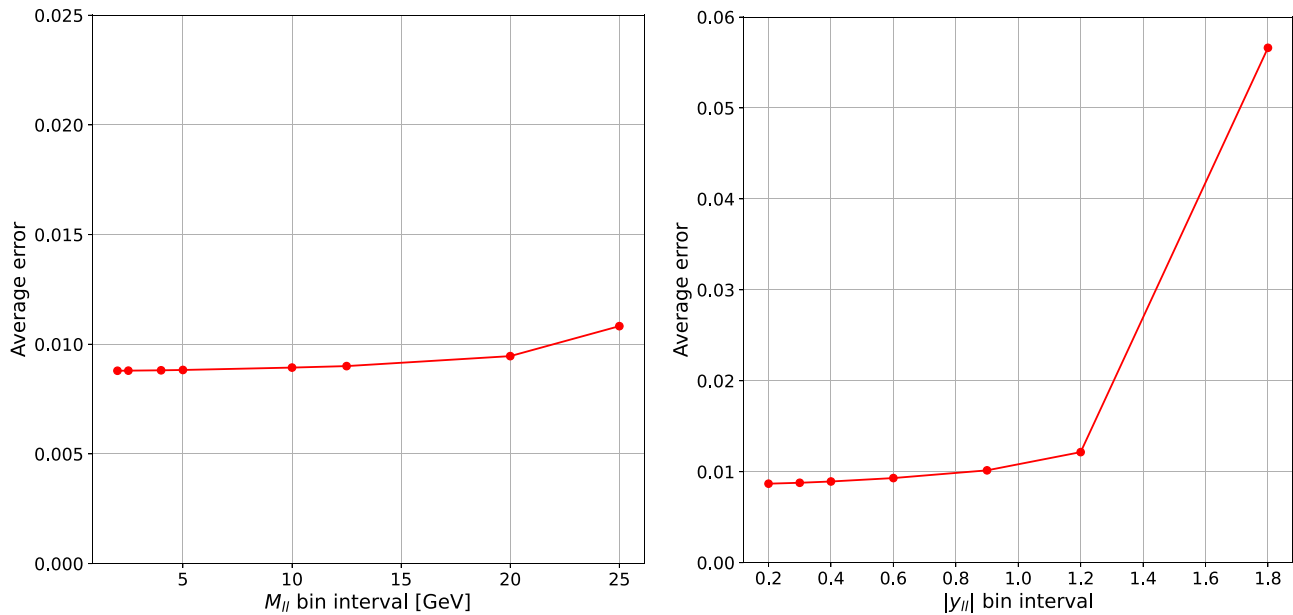


Fig. 6 The average error in the fitted couplings as a function of the invariant mass (left) and rapidity (right) bin widths

Table 1 The binning scheme used in our analysis

Observable	Bin boundaries
$M_{\ell\ell}$ [GeV]	45, 50, 55, 60, 65, 70, 75, 80, 85, 90, 95, 100, 105, 110, 115, 120, 125, 130, 135, 140, 145
$ y_{\ell\ell} $	0, 0.6, 1.2, 1.8, 2.4, 3.0, 3.6

scale process, and the calculation is performed in the $n_f = 5$ flavour scheme. The input theoretical parameters are chosen to be the ones from the EW G_μ scheme, which minimizes the impact of NLO EW corrections, see e.g. Ref. [55]. The explicit values for the relevant parameters in our analysis are the following: $M_Z = 91.188$ GeV, $\Gamma_Z = 2.441$ GeV, $M_W = 80.149$ GeV, $\alpha_{em} = 1/132.507$.

The predicted A_{FB} as a function of the invariant mass and rapidity of the di-lepton system at LO in the SM is shown in Fig. 1. The A_{FB} crosses zero around $M_{\ell\ell} \approx M_Z$. Also, due to its definition using the longitudinal boost of the di-lepton system, it approaches zero at $y_{\ell\ell} = 0$. For this calculation, we used the HERAPDF2.0 [16] PDF set, however, its general features do not depend on the PDF set.¹ We do not include any QED effects in our calculation since the experimental data are typically corrected for QED effects, and the uncertainties in these corrections are much smaller than the PDF uncertainties in A_{FB} [3].

We next investigate the dependence of the predicted A_{FB} on the couplings. In Figs. 2 and 3 we show the numerically-

¹ Theoretical predictions for A_{FB} obtained using other PDF sets can be found e.g. in Ref. [3] or Ref. [7].

calculated partial derivatives of the A_{FB} with respect to each coupling as a function of the invariant mass and rapidity of the dilepton system. Furthermore, in Figs. 4 and 5 these derivatives are shown with respect to the axial and vector couplings. It is instructive to see from Fig. 2 that the partial derivatives as functions of $M_{\ell\ell}$ cross zero at values of $M_{\ell\ell}$ which are almost independent of $y_{\ell\ell}$. As a result, the partial derivatives as functions of $y_{\ell\ell}$ vanish after integrating over the $M_{\ell\ell}$ regions which contain such turnover points near their centers (e.g., $\partial A_{FB}/\partial \delta g_R^{Zd} \approx 0$ for $85 < M_{\ell\ell} < 95$ GeV). This is an important observation for experimental analyses which aim to measure A_{FB} in bins of $M_{\ell\ell}$ and $y_{\ell\ell}$: in particular, in order to retain sensitivity to the couplings, the binning scheme should be chosen carefully, preferably such that the points where the derivatives vanish are placed at the bin boundaries, rather than at their centers. Furthermore, the magnitudes of the derivatives give an idea of which phase-space regions are expected to be most sensitive to the couplings. However, one needs to take into account the expected statistical uncertainties also. Therefore, we will come back to this after introducing the pseudodata in the next section.

3 Generation of pseudodata sets

Suitable data files which mimic future measurements at the HL-LHC have been generated for the analysis. Namely, we used the expected HL-LHC luminosity, SM theoretical predictions and our assumption of 20% for the detector response to predict the number of events and statistical uncertainties for the future A_{FB} measurement at the HL-LHC. The central

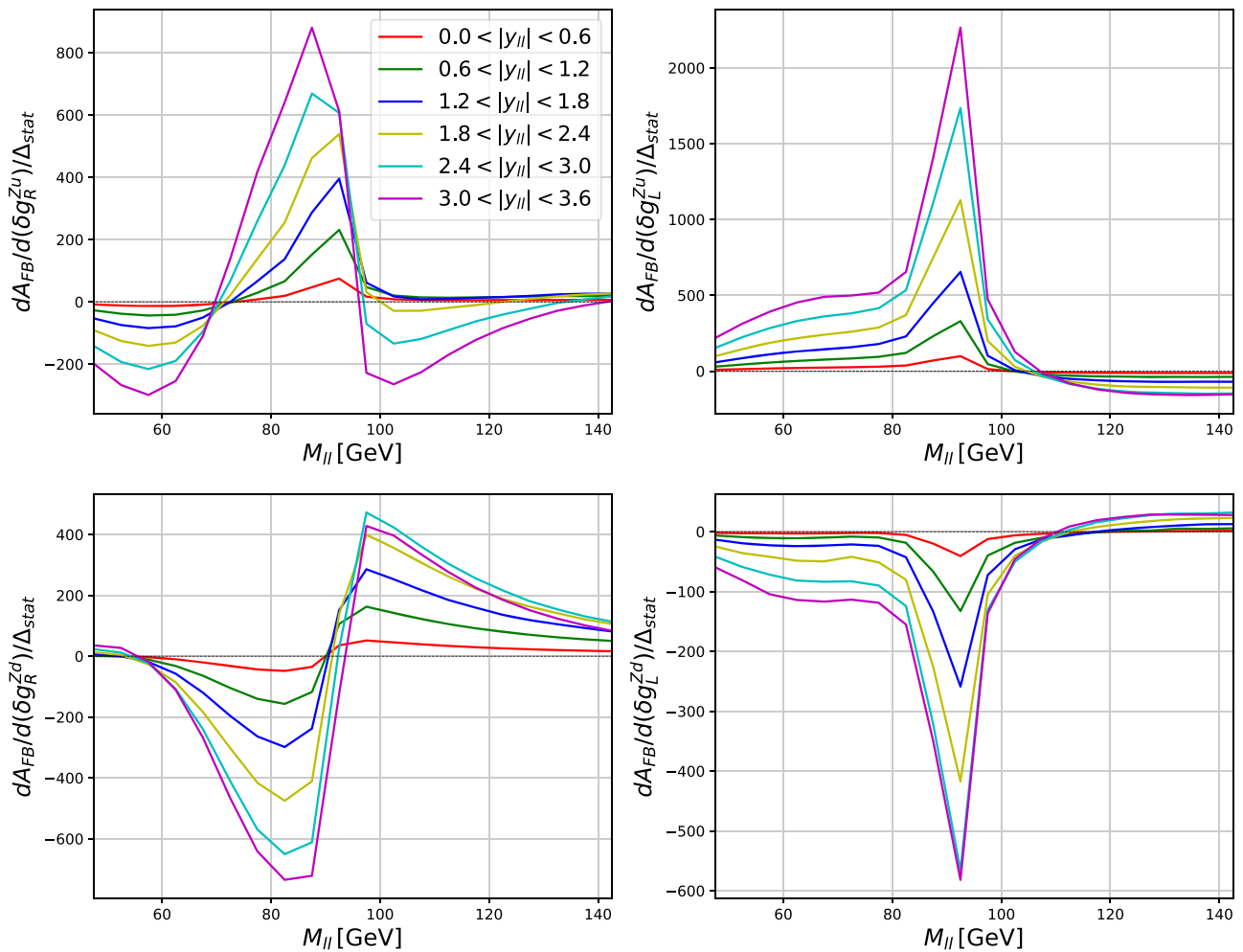


Fig. 7 The partial derivatives of the predicted A_{FB} with respect to δg_R^{Zu} (upper left), δg_L^{Zu} (upper right), δg_R^{Zd} (lower left) and δg_L^{Zd} (lower right) couplings weighted by the inverse of the statistical uncertainty as a function of the invariant mass of the dilepton system in different rapidity intervals at LO

values of the pseudodata points are set to the SM theoretical predictions. An important piece of information contained in the data files is the statistical precision associated to the A_{FB} experimental measurements in each bin. It is given by:

$$\Delta A_{FB} = \sqrt{\frac{1 - A_{FB}^2}{N}}, \quad (10)$$

where N is the expected total number of events in a specific invariant mass interval. We use the number of events with electron pairs from Z decays as predicted at LO with the acceptance cuts $|\eta_\ell| < 5$ and $p_T^\ell > 20$ GeV and introduce a further correction factor of 20% to model a realistic detector response [56]. The choice of LO accuracy for the expected number of events provides a conservative estimation of the statistical uncertainty. The higher-order QCD corrections through next-to-next-to-leading order (NNLO) for

the DY process are, generally, moderate and do not distort much differential distributions, see, e.g. Ref. [57]. We have checked that the usage of NNLO QCD predictions would increase the expected number of events by factor 1.1–1.4 depending on the phase space region, so the statistical uncertainties does not change by more than 20% [9]. Furthermore, we have tested our approach by comparing the statistical uncertainties from the ATLAS measurement of A_{FB} [3] with the ones produced using our pseudodata scenario, and found a reasonable agreement within a factor of two.²

The pseudodata have been generated for the collider centre-of-mass energy of 13 TeV and integrated luminosity of 3000 fb^{-1} , the designed integrated luminosity at the end of the HL-LHC stage [51]. To explore different proton PDF sets,

² Since the results of the ATLAS measurement [3] are reported in the full phase space of the leptons, the statistical uncertainties depend also on the extrapolation factors which we did not include in this study.

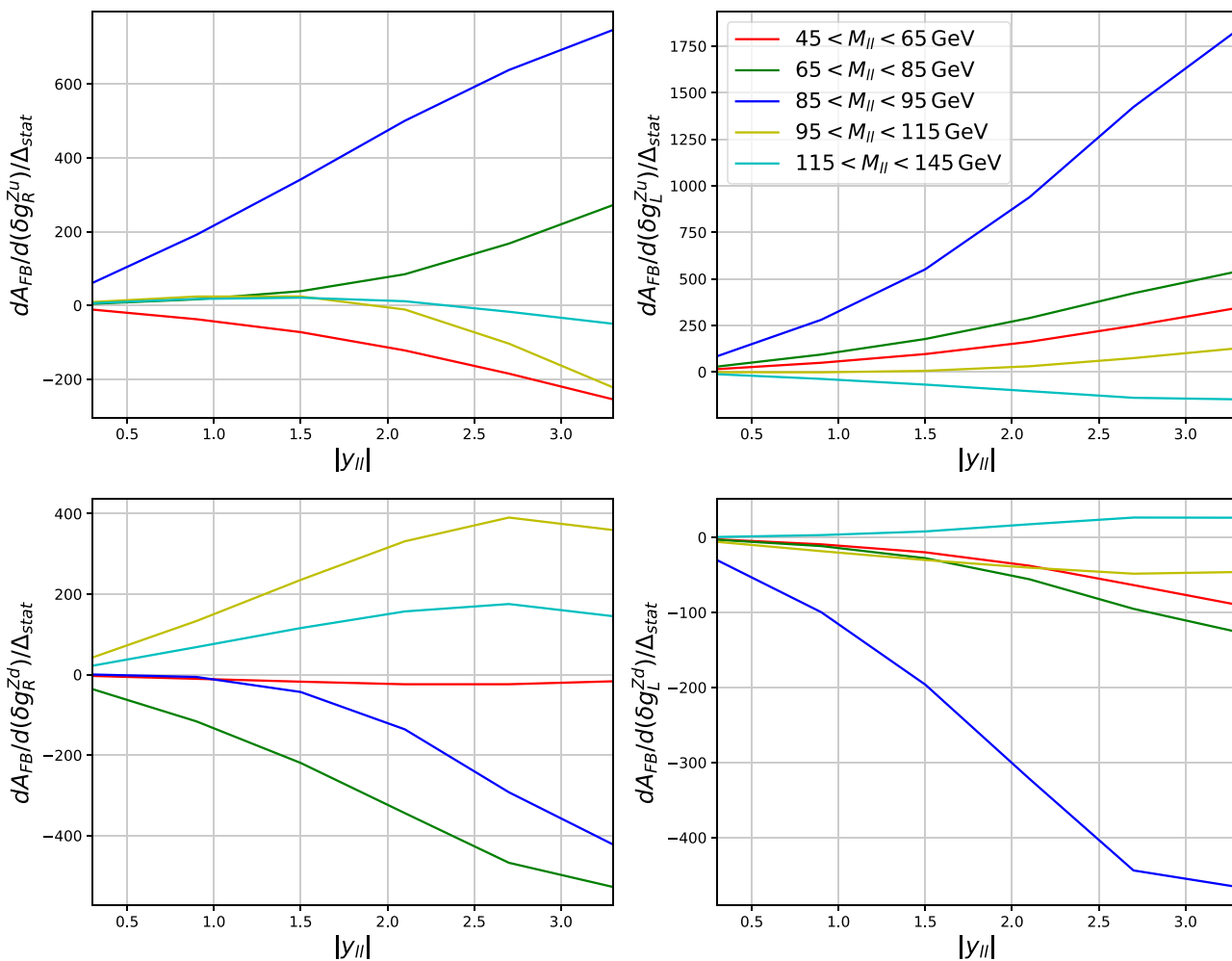


Fig. 8 The partial derivatives of the predicted A_{FB} with respect to δg_R^{Zu} (upper left), δg_L^{Zu} (upper right), δg_R^{Zd} (lower left) and δg_L^{Zd} (lower right) couplings weighted by the inverse of the statistical uncertainty as a function of the rapidity of the dilepton system in different invariant mass intervals at LO

several data files have been generated adopting the recent NNLO variants of the PDF sets CT18 [12], NNPDF4.0 [14], ABMP16 [15], HERAPDF2.0 [16] and MSHT20 [13] along with their respective uncertainties as provided by each fitting group.

Theoretical uncertainties arising from the choice of factorization and renormalization scales have been assessed. For this purpose, we used theoretical predictions at NLO obtained using MadGraph5_aMC@NLO [58] interfaced to APPLgrid [59] through aMCfast [60]. We have found that the impact of scale variations by the conventional factor of two in the theoretical predictions at NLO is small compared to the statistical uncertainties of the pseudodata, and thus we do not include it in our analysis. A similar study (focused on the impact of the A_{FB} on PDFs) was performed in Ref. [9]. Also, it is worth mentioning that even smaller theoretical uncertainties could be expected at NNLO in QCD. Furthermore, while it would be important to include the NLO

EW effects in an analysis of experimental data aiming to obtain accurate central values, they are not expected to bring significant modification to the uncertainties.

Another important ingredient of the pseudodata is the binning scheme. As discussed in Sect. 2, bins with the turnover points of the partial derivatives of A_{FB} with respect to the couplings should be avoided, because in such bins the sensitivity to the couplings is washed out after integrating over the bin. In general, one needs as fine as possible bins in order to maximize the sensitivity to the parameters of interest. However, due to limited detector resolution too fine bins cannot be used. We have optimized the bin widths based on the precision of the fitted couplings which we extract from the pseudodata. As a figure of merit, we have used the geometrical average error of the couplings, i.e. the fourth root of the product of the resulting uncertainties on each of the four determined couplings, $\sqrt[4]{\Delta\delta g_R^{Zu} \Delta\delta g_R^{Zd} \Delta\delta g_L^{Zu} \Delta\delta g_L^{Zd}}$. In Fig. 6

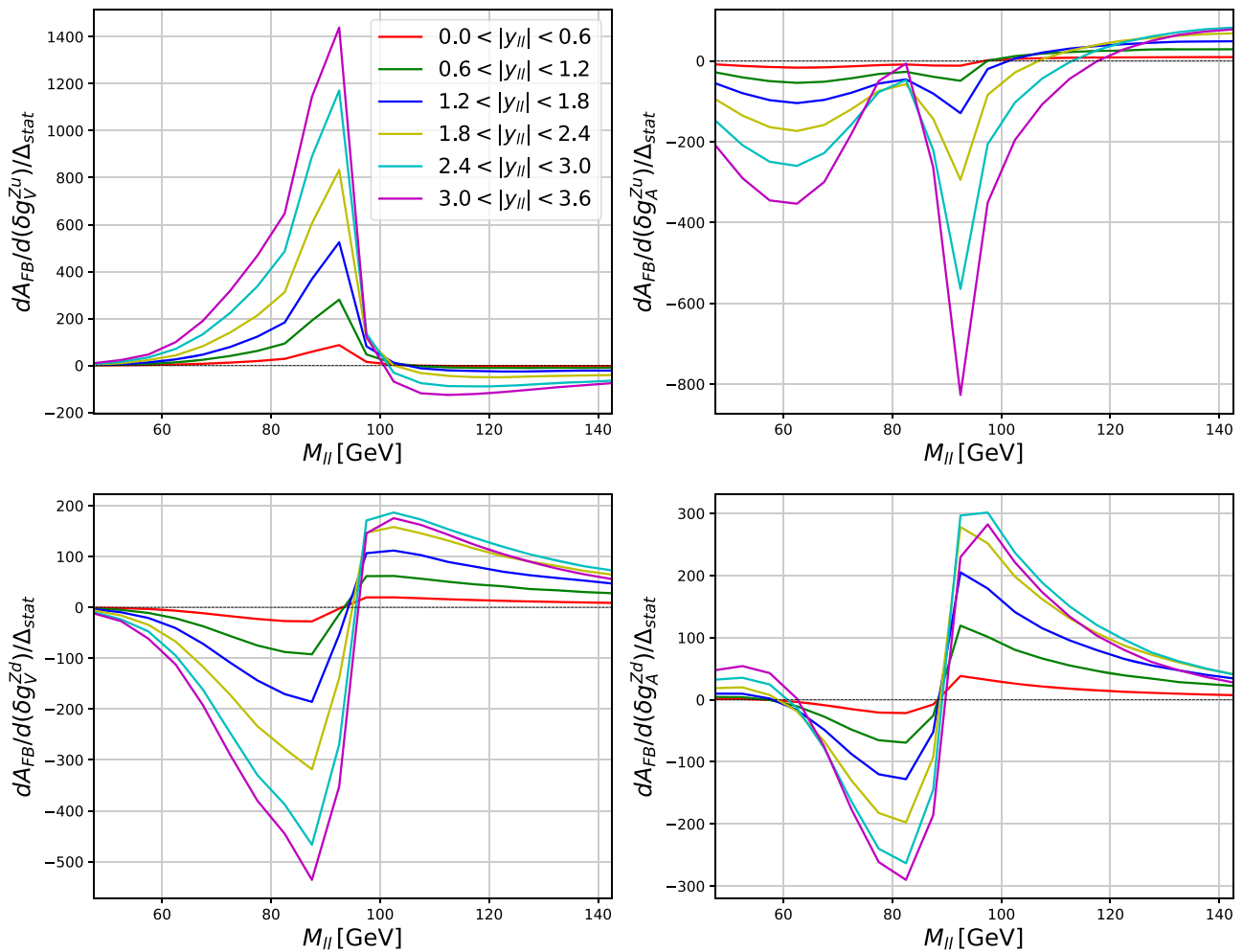


Fig. 9 Same as in Fig. 7 for the axial and vector couplings

we show this quantity as a function of the invariant mass and rapidity bin widths. Based on this study, we chose the bin width of 5 GeV in the invariant mass and 0.6 in the rapidity of the dilepton system, since a further reduction of the bin width does not improve the sensitivity to the couplings significantly. Namely, using the 10 GeV bin width in M_{ll} , one will get about 1% larger uncertainties on the fitted couplings than using the 5 GeV bin width, which we find already sizeable. On the other hand, using a smaller bin width < 5 GeV provides only a marginal further improvement at permil level. These bin widths are feasible given the resolution of the existing detectors [61, 62]. The minimum expected number of events in a bin amounts to $\sim 10,000$, thus the probability distribution function of the statistical uncertainty is well approximated by a normal distribution. Our binning scheme is given in Table 1.

It is illustrative to look at the magnitudes of the partial derivatives as a function of the invariant mass and rapidity of the dilepton system weighted by the inverse of the statistical uncertainty of pseudodata in the corresponding phase-space region, as shown in Figs. 7, 8, 9 and 10. This quantity is proportional to the sensitivity to the couplings which can be extracted from such a phase-space region. The largest sensitivity to the couplings is expected in the region $55 \lesssim M_{ll} \lesssim 110$ GeV (see Figs. 7, 9), and in our analysis we have adopted a slightly wider range $45 < M_{ll} < 145$ GeV. Possible contributions from four-fermion operators in this kinematic range are expected at the $\lesssim 1\text{‰}$ level [41]. As a simplifying assumption, we neglected them in our analysis. A study of their possible impact is described in Appendix A.

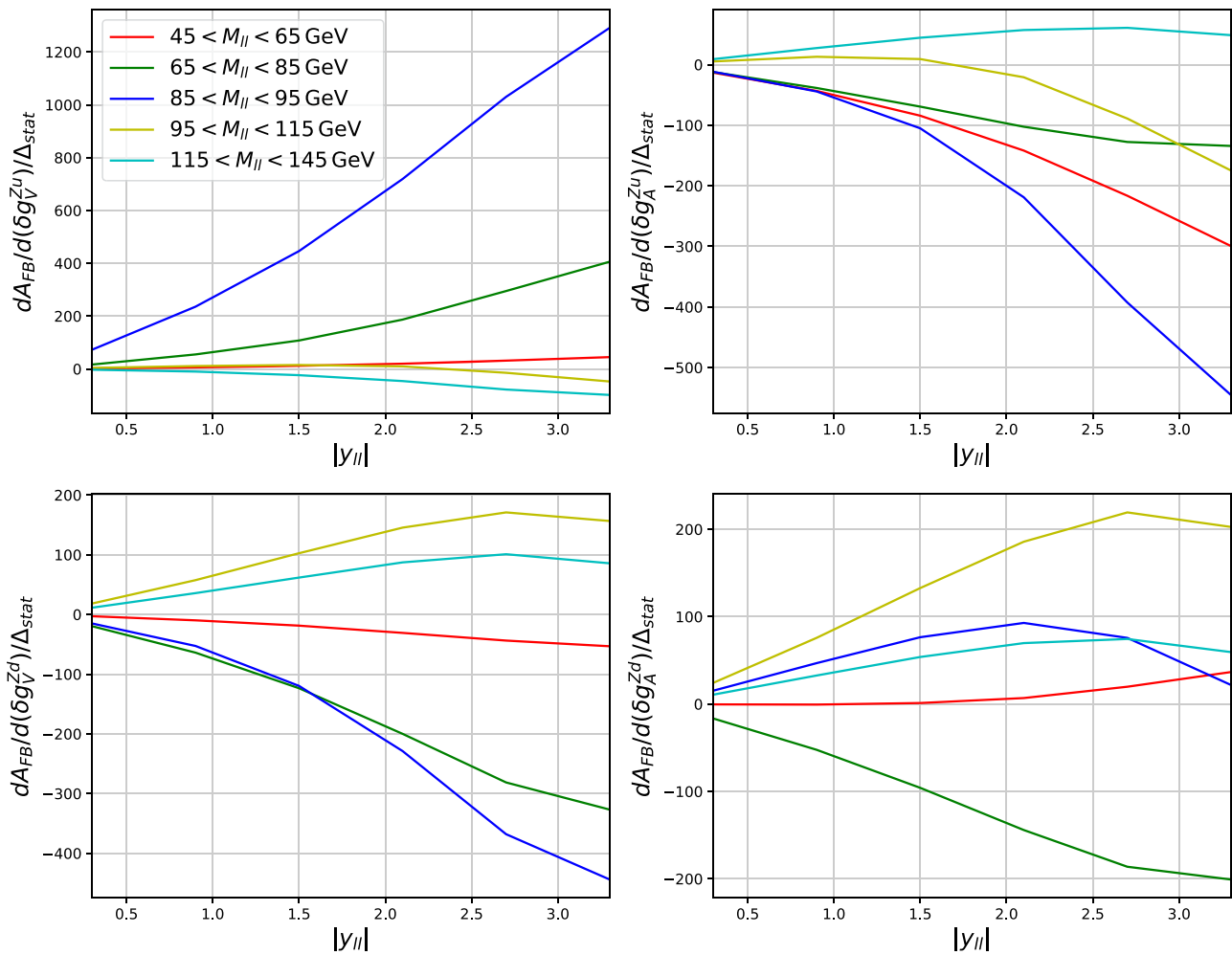


Fig. 10 Same as in Fig. 8 for the axial and vector couplings

We have limited the rapidity region $|y_{||}| < 3.6$ assuming the extension of the detector acceptance up to pseudorapidity $|\eta| < 5$ (while potentially the region $|y_{||}| > 3.6$ could provide even further improvement for the sensitivity to the couplings).

4 Results

The pseudodata sets are fitted with the four modifications to the couplings δg_L^{Zu} , δg_R^{Zu} , δg_L^{Zd} , δg_R^{Zd} being free parameters. The fit is performed using the MINUIT [63] library by minimizing a χ^2 expression:

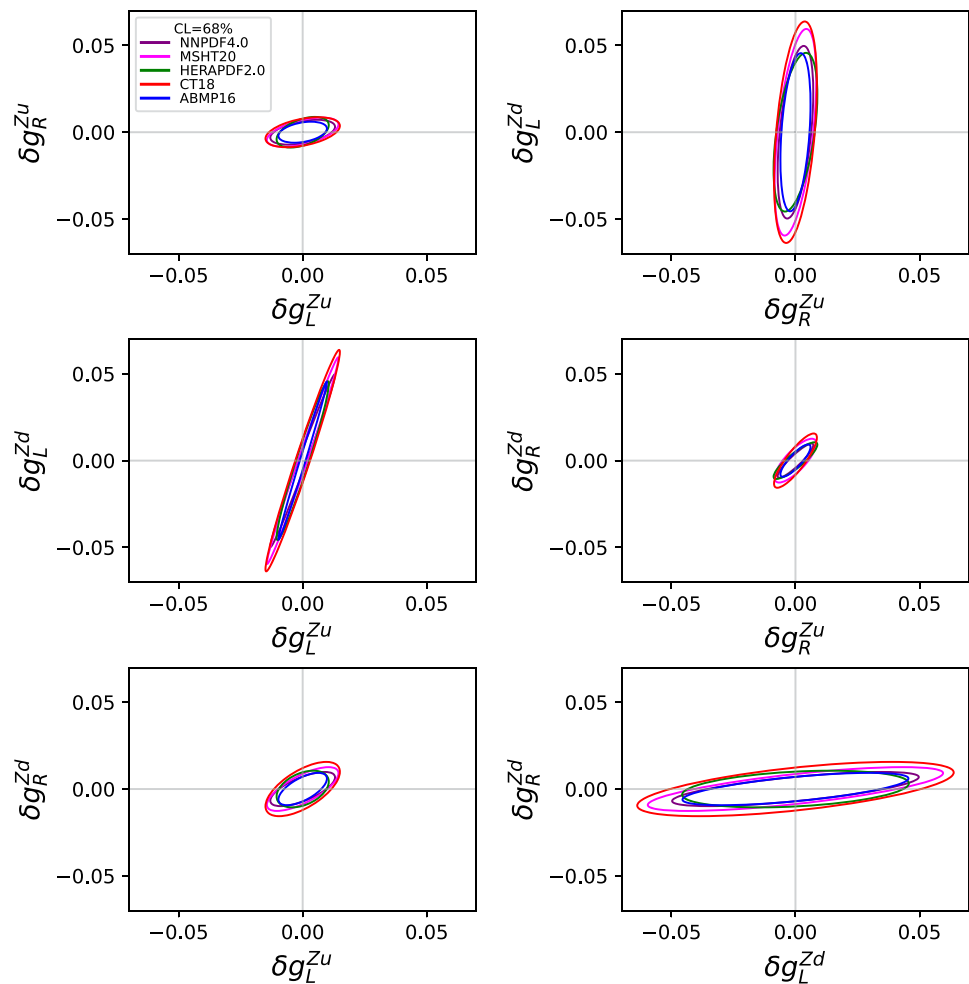
$$\chi^2 = \sum_i \frac{(m^i - \sum_j \gamma_j^i m^i s_j - \mu_i)^2}{\delta_i^2} + \sum_j s_j^2, \tag{11}$$

which follows the one used in Ref. [16]. Here, μ^i is the measured value in bin i , δ_i is its experimental uncertainty, m^i is

the theoretical prediction, γ_j^i is its relative uncertainty due to the PDF eigenvector j which is shifted in units of sigma by s_j . The γ_j^i relative uncertainty is calculated for each bin i by taking the difference between the theoretical prediction obtained using the j -th PDF eigenvector³ and the nominal theoretical prediction obtained using the central PDF set, and dividing this difference by the nominal prediction. This treatment of the PDF uncertainties follows the so-called profiling technique [64,65]. In this method, the PDF uncertainties are included in the χ^2 using nuisance parameters s_j which are further constrained according to the tolerance criterion of the fit. The number of nuisance parameters s_j corresponds to the number of eigenvectors for each PDF set. While s_j are free parameters when minimizing the χ^2 , they do not change the

³ We convert the uncertainties of the NNPDF4.0 set which are provided using a Monte Carlo representation with replicas to Hessian eigenvectors. Furthermore, we have checked, that we obtain identical results if using the corresponding NNPDF set with Hessian eigenvectors (NNPDF40_nnlo_as_01180_hessian) directly.

Fig. 11 Allowed regions for all pairs of corrections to the Z couplings to u - and d -type quarks obtained using different PDF sets



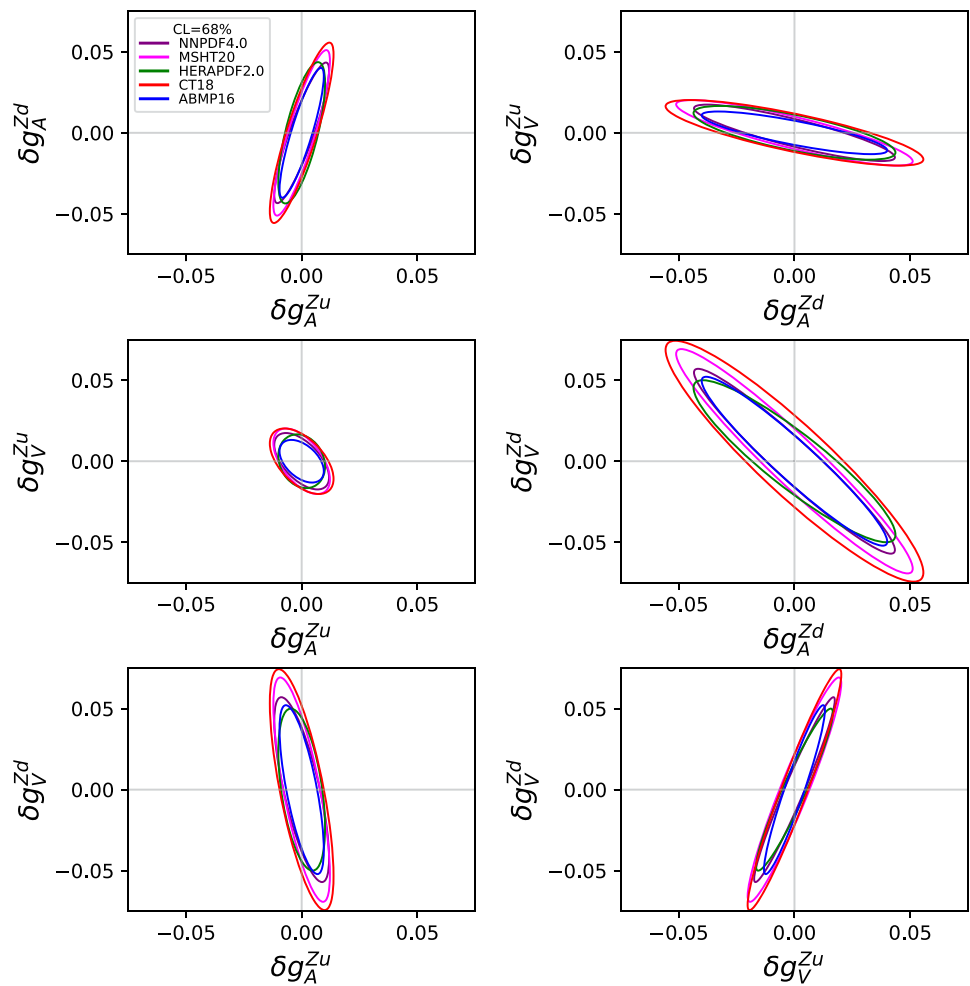
number of degrees of freedom, because for each s_j the corresponding prior is added, represented by the last term in Eq. (11), which acts as a data point. As the tolerance criterion we use $\Delta\chi^2 = 1$. In this approach, one assumes that the new data are compatible with the theoretical predictions using the existing PDF set. No further theoretical uncertainties beyond the PDF uncertainties are considered when calculating the χ^2 . The uncertainties on the fitted parameters are obtained using the HESSE method which computes numerically the second derivatives of the χ^2 with respect to the fitted parameters [48,50]. This assumes that the dependence of the theoretical predictions on the parameters of interest is linear near the minimum of the χ^2 . We cross-checked the uncertainties using the MINOS algorithm which uses the profile likelihood method to compute asymmetric confidence intervals, as well as the MNCENT algorithm [63] which explicitly finds 2D contours where the χ^2 is minimal, and found a good agreement with the hessian uncertainties.

The results of the fit are presented in Figs. 11, 12, 13, 14, 15, 16, 17, 18 and 19 as allowed regions for different pairs

of corrections to the Z couplings to u - and d -type quarks at confidence level (CL) of 68%.⁴ Note that we fit four couplings at a time, while for presentation purposes we show 2D projection plots with different pairs of couplings. The resulting uncertainties on the couplings to the d -type quarks are roughly a factor of two larger than the corresponding uncertainties for the u -type quarks. A similar impact of the A_{FB} measurements on the PDFs was found in Ref. [9]: it was shown that these measurements are most sensitive to the weighted sum $(2/3)u_v + (1/3)d_v$ of the valence u - and d -quarks, and we report the same finding in the present study. This is related to the valence quark content of the proton and also to the fact that the $d\bar{d}$ initiated process gets more suppressed at high rapidity (where the sensitivity to the couplings is largest) in comparison to the $u\bar{u}$ initiated ones [8]. The exact details of this effect depend on the quark PDF behaviour at high values of the partonic momentum fraction

⁴ To plot the allowed regions for each pair of the corrections to the Z couplings, we use the $\Delta\chi^2 = 2.3$ criterion which is appropriate for joint estimation of two parameters.

Fig. 12 Same as in Fig. 11 for the axial and vector couplings



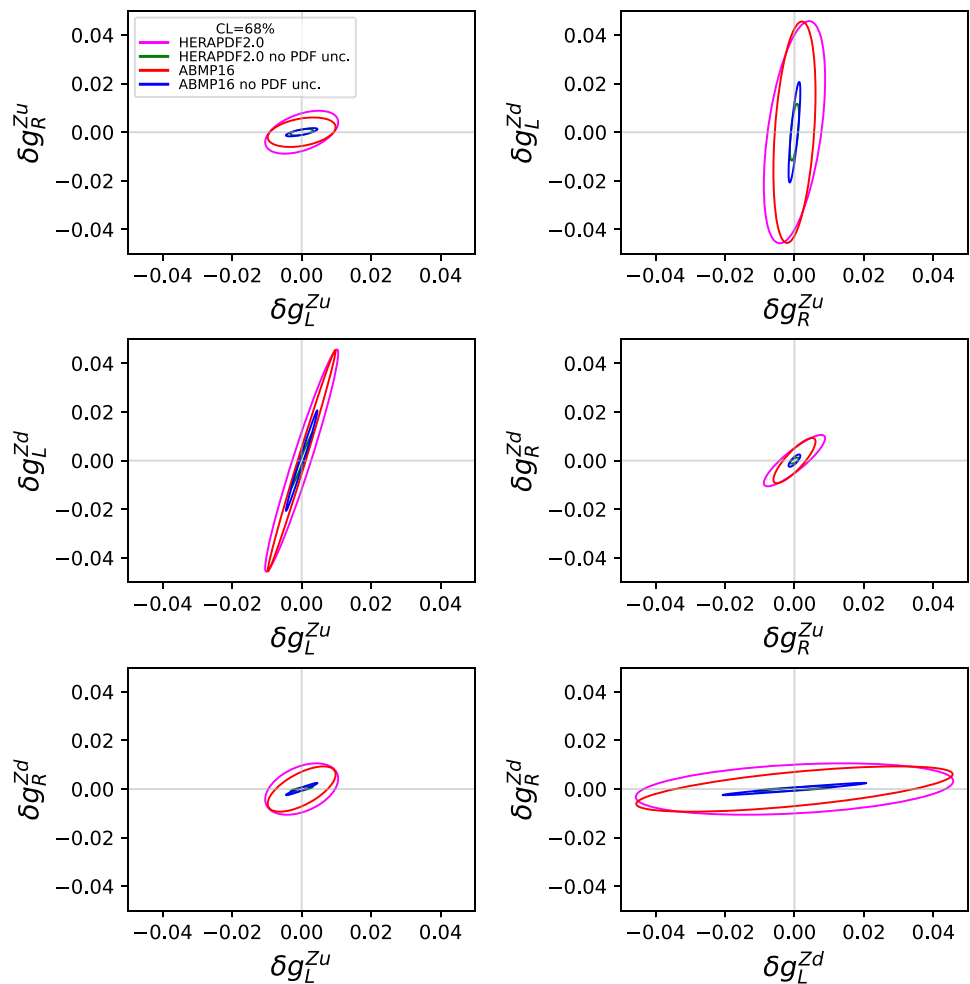
x [17,24,25,46,66]. We find a strong correlation (up to 0.95) between the different couplings, as illustrated in Figs. 11, 12, 13, 14, 15, 16, 17, 18 and 19, while the correlation coefficients between the couplings and the quark PDFs are moderate (about 0.5). Furthermore, the latter exhibit significant variability across different values of x , reflecting the complex correlation of the different parton distributions in the original PDF sets.

In Figs. 11 and 12 the allowed regions are shown as obtained using different PDF sets.⁵ These results are presented using either couplings to right- and left-handed quarks or axial-vector couplings. Both the size and the shape of the allowed regions (i.e. the correlations between the fitted parameters) are similar, independent of the PDF set. To illustrate the impact of the PDF uncertainties on the results, in Figs. 13 and 14 we show the allowed regions obtained with and without including the PDF uncertainties into the fit. Furthermore, in Fig. 15 we show the average size of the uncertainties on the fitted couplings as obtained using different

PDF sets. The impact of the PDF uncertainties is sizable. Namely, after including them into the fit the uncertainties on the couplings increase by a factor of ~ 3 , i.e. the resulting uncertainties on the couplings are dominated by the PDF uncertainties. When using different PDF sets, the size of the average uncertainty does not change by more than a factor of 1.5 indicating a reasonable consistency between the size of the PDF uncertainties for the modern PDF sets. However, it is worth mentioning also that the PDF uncertainties are constrained by the pseudodata when using the profiling technique. The behaviour of quark and antiquark densities at large Bjorken- x varies significantly between different PDF sets [7,8,17] strongly affecting the theoretical predictions for the A_{FB} in the high rapidity bins. However the discrepancies between different PDF sets will foreseeably reduce after the inclusion of additional experimental data covering the large- x regions [66]. The A_{FB} observable has proved particularly sensitive to quark and anti-quark densities in the large Bjorken- x region [9,11,17], which can be accessed through measurements of the asymmetry at high rapidities [9,11]. In

⁵ The PDF uncertainties of the CT18 set were rescaled to CL=68%.

Fig. 13 Allowed regions for all pairs of corrections to the Z couplings to u - and d -type quarks obtained using the ABMP16 and HERAPDF2.0 PDF sets with and without PDF uncertainties



order to provide consistent results, in the future such analyses should comprise a simultaneous fit of the proton PDFs and the couplings.

In Figs. 16 and 17 we compare our results obtained for the HL-LHC⁶ with the other analyses of existing data from LEP, Tevatron, HERA and LHC. The results are presented using either couplings to right- and left-handed quarks or axial and vector couplings. Namely, we compare with the analysis of the H1 Collaboration at HERA [67], the LEP+SLD combination [5], the analysis of D0 Collaboration at Tevatron [68] and the analysis of LEP, ATLAS and D0 data from Ref. [43].⁷ In addition to the HL-LHC results, we present our results

⁶ We show the results obtained using the ABMP16 PDF set, since only this set provides symmetric PDF errors which are easier to include in the PDF profiling.

⁷ Note that on these plots we compare published results, which are obtained with different methodology in some cases. E.g. in our work and Refs. [69,70] the assumption $\delta g_{R,L}^{Zd} = \delta g_{R,L}^{Zs} = \delta g_{R,L}^{Zb} = \delta g_{R,L}^{Zu} = \delta g_{R,L}^{Zc}$ was used, while in Ref. [43] the couplings to quarks of different flavours were fitted separately. Also, Refs. [5] and [43] differ in the treatment of higher-order interference effects between the SM and new physics,

of analyzing all available 10 bins from the ATLAS measurement of A_{FB} [3], while only 4 bins at the Z peak were used in the analysis of Ref. [43]. For the analysis of ATLAS data, we set the central data points to the theoretical predictions obtained at LO, while we use the data statistical and systematic uncertainties, as well as the PDF uncertainties. The analysis of ATLAS data follows the procedure used for the HL-LHC pseudodata. Such a procedure provides credible uncertainties on the Z couplings, while in order to get meaningful central values one would need to use theoretical calculations with higher-order QCD corrections. Given that the experimental uncertainties of the ATLAS data are larger than the uncertainties of the HL-LHC pseudodata, the PDF uncertainties play a moderate role in this case. The level of precision expected at the HL-LHC outperforms any existing data sets [5,43,67,68,71,72]. Also, we note that using all the 10 data bins from the ATLAS measurement [3] provides more information on some of the couplings (e.g. δg_R^{Zd}) com-

universality assumption for down-type quarks, and the number of fitted parameters.

Fig. 14 Same as in Fig. 13 for the axial and vector couplings

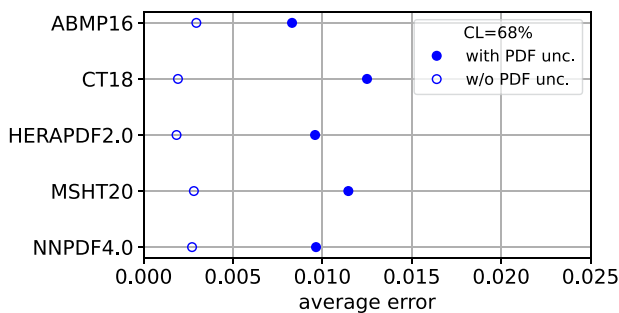
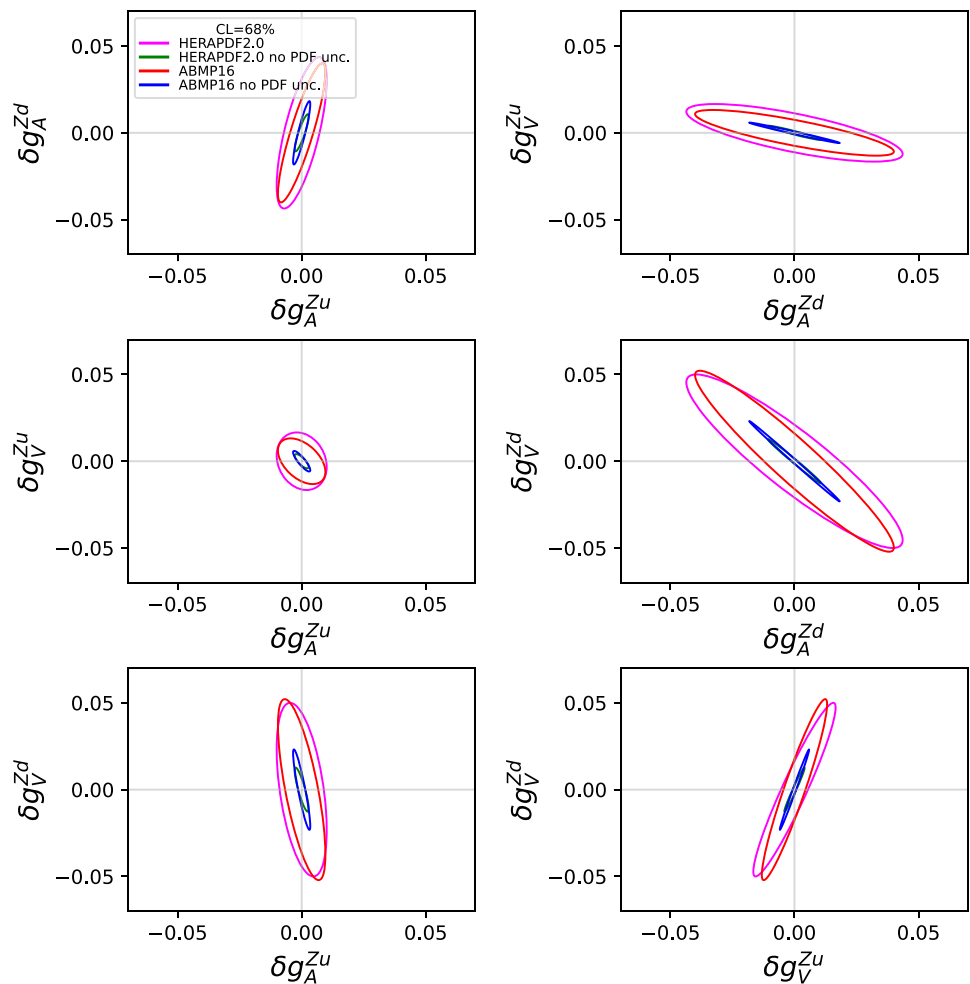


Fig. 15 The average size of the uncertainties on the fitted corrections to the Z couplings to *u*- and *d*-type quarks obtained using different PDF sets

pared to the 4 bins at the *Z* peak together with the LEP and D0 data which were used in the analysis of Ref. [43].

In Figs. 18 and 19 we compare the results obtained for the HL-LHC with the results expected at the future colliders currently under discussion, LHeC [69,73] and FCC-eh [70,74]. For the LHeC, two electron beam energies of 50 or 60 GeV

are considered, and two assumptions on the uncertainties. The results are provided for the so-called aggressive uncertainty scenario for $E_e = 60$ GeV, and the conservative one for $E_e = 50$ GeV (further details can be found in Ref. [69]). Furthermore, in Fig. 20 the average size of the uncertainties which can be obtained using current and future data sets are compared. A sub-percent level of precision is expected at the LHeC, FCC-eh and HL-LHC, which is one order of magnitude better than what can be obtained using existing data sets from LEP, Tevatron, HERA and LHC. More precisely, the average size of the uncertainties which are expected at the FCC-eh are a factor of 6 better than the one from our HL-LHC expectation, while the LHeC uncertainties are only 1.7–4 times smaller (depending on the scenario) than our HL-LHC results. Note that uncertainties may be also reduced at FCC-hh collider, due to increased cross section and luminosity compared to the HL-LHC. This could be studied using similar methods as those used for the HL-LHC in this paper. However, it requires a dedicated investigation of the detector acceptance and is beyond the scope of the current analysis.

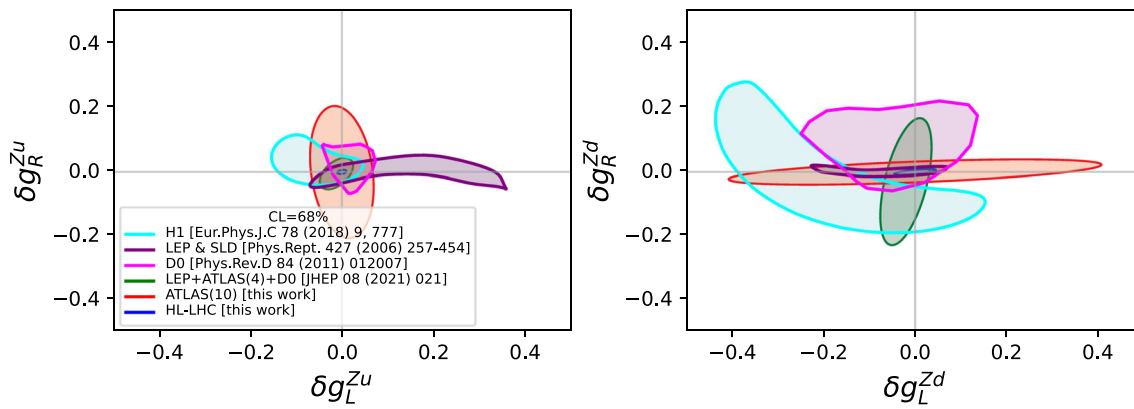


Fig. 16 Allowed regions for all pairs of corrections to the Z couplings to u - and d -type quarks obtained using HL-LHC pseudodata as well as different existing data sets

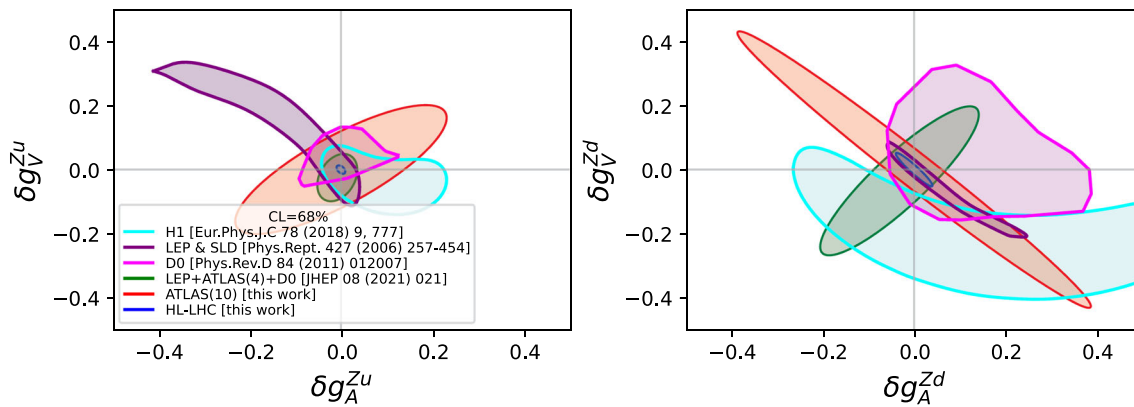


Fig. 17 Same as in Fig. 16 for the axial and vector couplings

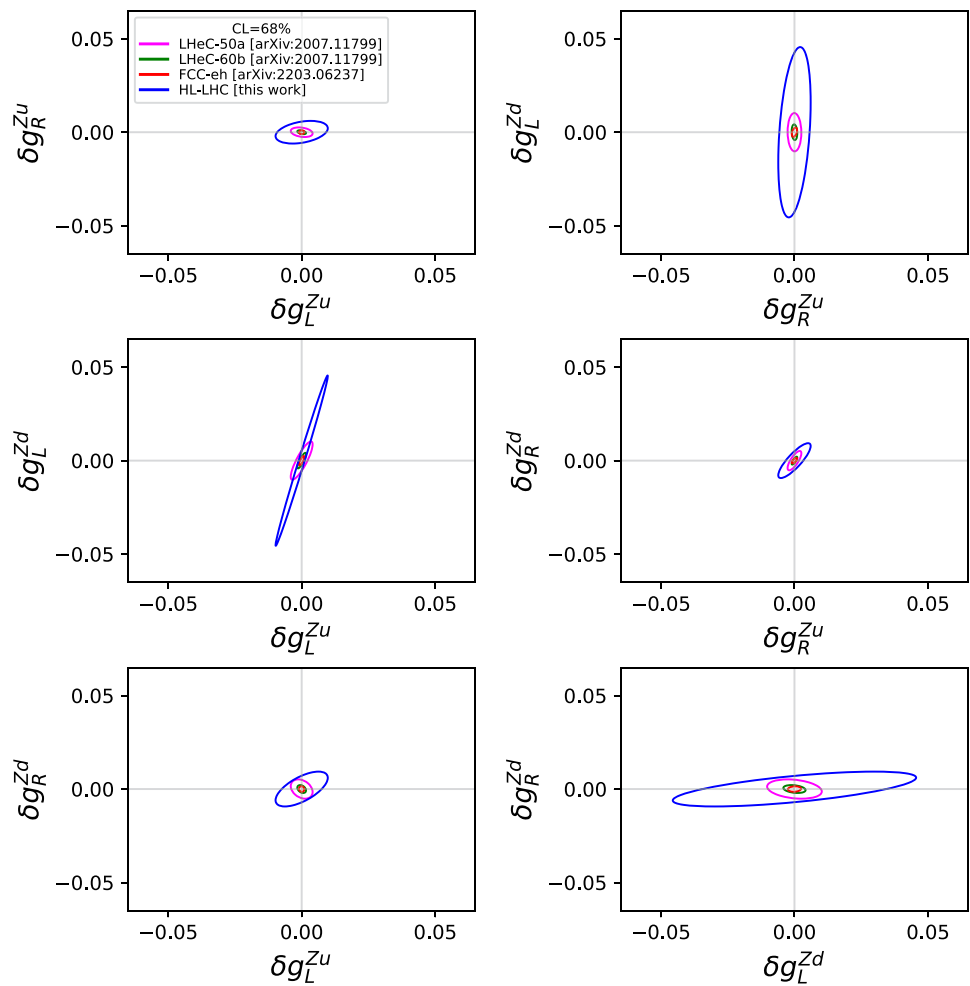
5 Conclusions

We have studied the possibility to improve constraints on the Z couplings to the u - and d -type quarks using the future measurements of A_{FB} at the HL-LHC with 3000 fb^{-1} . We have investigated in detail the dependence of the A_{FB} on the various couplings in different regions of the invariant mass of the lepton pair, and we have shown that a wide range of $45 < M(l\bar{l}) < 145 \text{ GeV}$ is profitable to constrain the couplings. Furthermore, a measurement as function of the rapidity of the lepton pair provides a significant added value. Thus, we suggest double-differential measurements of the A_{FB} as a function of both the invariant mass and rapidity of the lepton pairs, as done e.g. in Refs. [3,43]. Our quantitative

analysis of the impact of the binning scheme on the precision of the extracted couplings suggests the choice of a specific binning scheme which ensures a substantial sensitivity to the couplings in such a measurement.

The resulting uncertainties on the couplings to the d -type quarks are found to be approximately a factor of two larger than the corresponding uncertainties for the u -type quarks. Since the A_{FB} observable is strongly sensitive to the proton PDFs, we find a significant dependence of the results on the PDF set used for such study, as was checked using the ABMP16, CT18, HERAPDF2.0, MSHT20 and NNPDF4.0 PDF sets. Preferably, in the future such analyses should comprise a simultaneous fit of the proton PDFs and the couplings.

Fig. 18 Allowed regions for all pairs of corrections to the Z couplings to u - and d -type quarks obtained using HL-LHC pseudodata compared to the ones for different future experiments



The results were compared with the existing analyses of the LEP, HERA, Tevatron and LHC data, as well as with the results which are expected at the future colliders LHeC and FCC-eh. The uncertainties on the Z couplings to the u - and d -type quarks at the HL-LHC are expected at percent level,

thus outperforming by an order of magnitude any determinations of these couplings using existing data sets. This level of precision is similar, but a little inferior to the one which is expected at the LHeC and FCC-eh.

Fig. 19 Same as in Fig. 18 for the axial and vector couplings

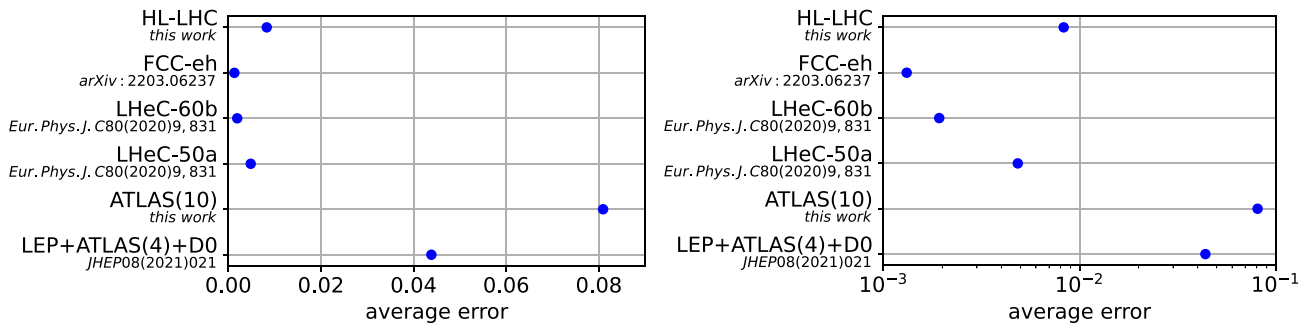
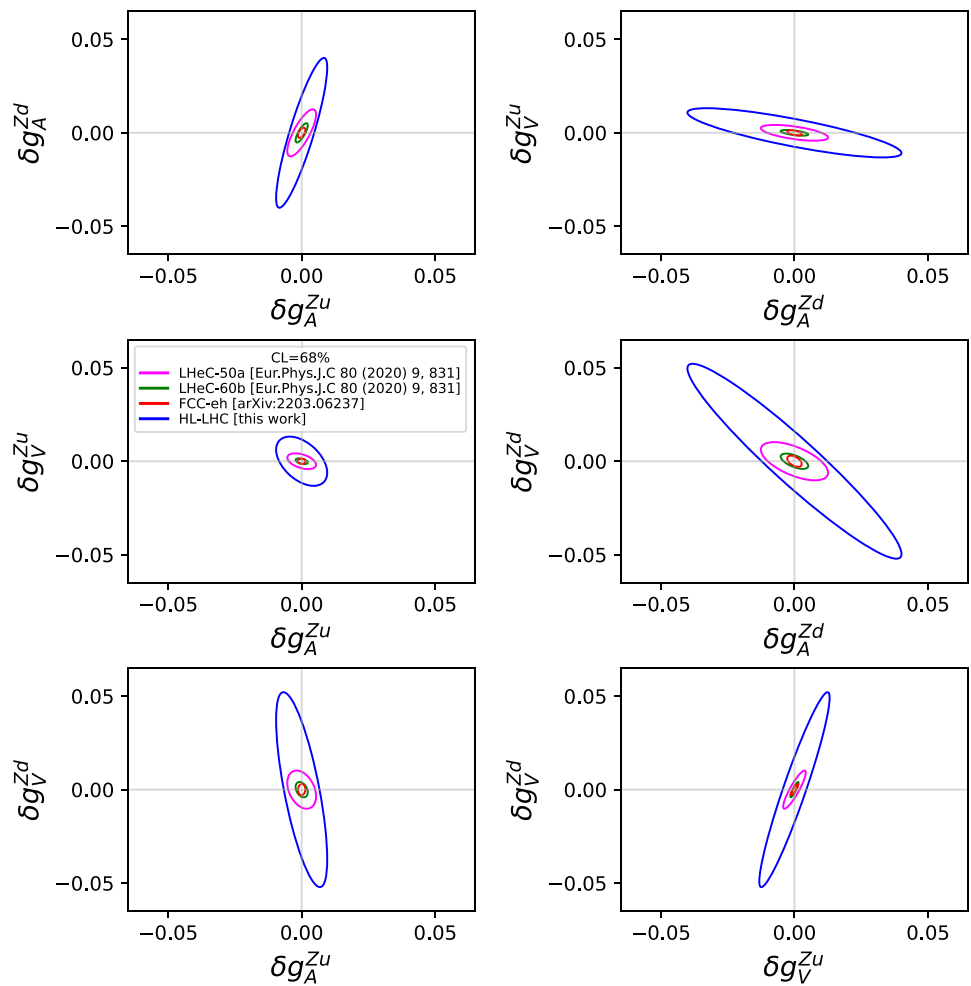


Fig. 20 The average size of the uncertainties on the fitted corrections to the Z couplings to *u*- and *d*-type quarks for different future experiments using the linear (left) or logarithmic (right) scale

Acknowledgements The work of S. M. has been supported in part by the Bundesministerium für Bildung und Forschung under contract 05H21GUCCA. The work of O. Z. has been supported by the *Philipp Schwartz Initiative* of the Alexander von Humboldt foundation. We thank Radja Boughezal and Yingsheng Huang for providing predictions for the SMEFT contributions of the four-fermion operators to A_{FB} . We thank Adam Falkowski for the valuable comments on the comparison of the results from Refs. [5,43].

Data Availability Statement This manuscript has no associated data. [Author’s comment: Data sharing not applicable to this article as no datasets were generated or analysed during the current study.]

Code Availability Statement This manuscript has no associated code/software. [Author’s comment: Code/Software sharing not applicable to this article as no code/software was generated or analysed during the current study.]

Open Access This article is licensed under a Creative Commons Attribution 4.0 International License, which permits use, sharing, adaptation, distribution and reproduction in any medium or format, as long as you give appropriate credit to the original author(s) and the source, provide a link to the Creative Commons licence, and indicate if changes were made. The images or other third party material in this article are included in the article’s Creative Commons licence, unless indicated otherwise in a credit line to the material. If material is not included in the article’s Creative Commons licence and your intended use is not permitted by statutory regulation or exceeds the permitted use, you will need to obtain permission directly from the copyright holder. To view a copy of this licence, visit <http://creativecommons.org/licenses/by/4.0/>. Funded by SCOAP³.

Appendix A: Study of the impact of four-fermion SMEFT operators

While the vertex corrections to the vector boson couplings to fermions scale as M_Z^2/Λ^2 , the four-fermion interactions scale as M_{ll}^2/Λ^2 and can be safely neglected on-peak, but potentially may become large at $M_{ll} > M_Z$. In Fig. 21 we compare the impact on A_{FB} of the linear contributions of two four-fermion operators $C_{lq}^{(1)}$ and C_{eu} from Ref. [41] with the impact of the vertex corrections to the couplings as a function of M_{ll} . For the four-fermion operators, the assumptions are $C = 1$ and $\Lambda = 4$ TeV as typically used in the literature [41], while for the vertex corrections we have varied the couplings by their uncertainties which were obtained in our study for the HL-LHC scenario with ABMP16 PDF set (see Fig. 11). As expected, the impact of the four-fermion operators is strongly suppressed at $M_{ll} \sim M_Z$, but it grows off-peak and becomes comparable to the impact of the vertex corrections to the couplings at $M_{ll} \approx 150$ GeV. Since in our analysis we have chosen the region $M_{ll} < 145$ GeV, we did not include the four-fermion operators.⁸

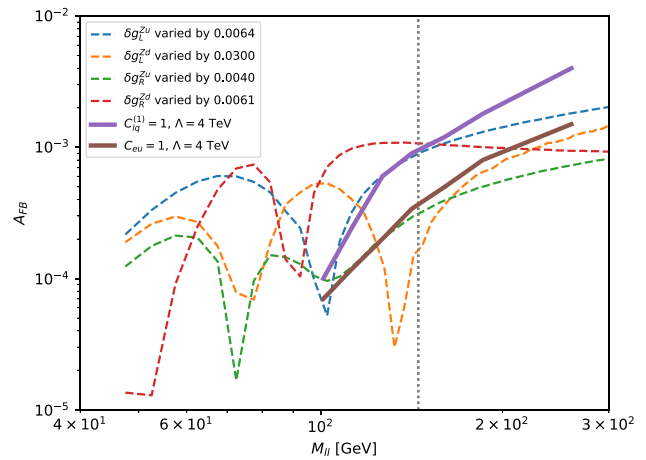
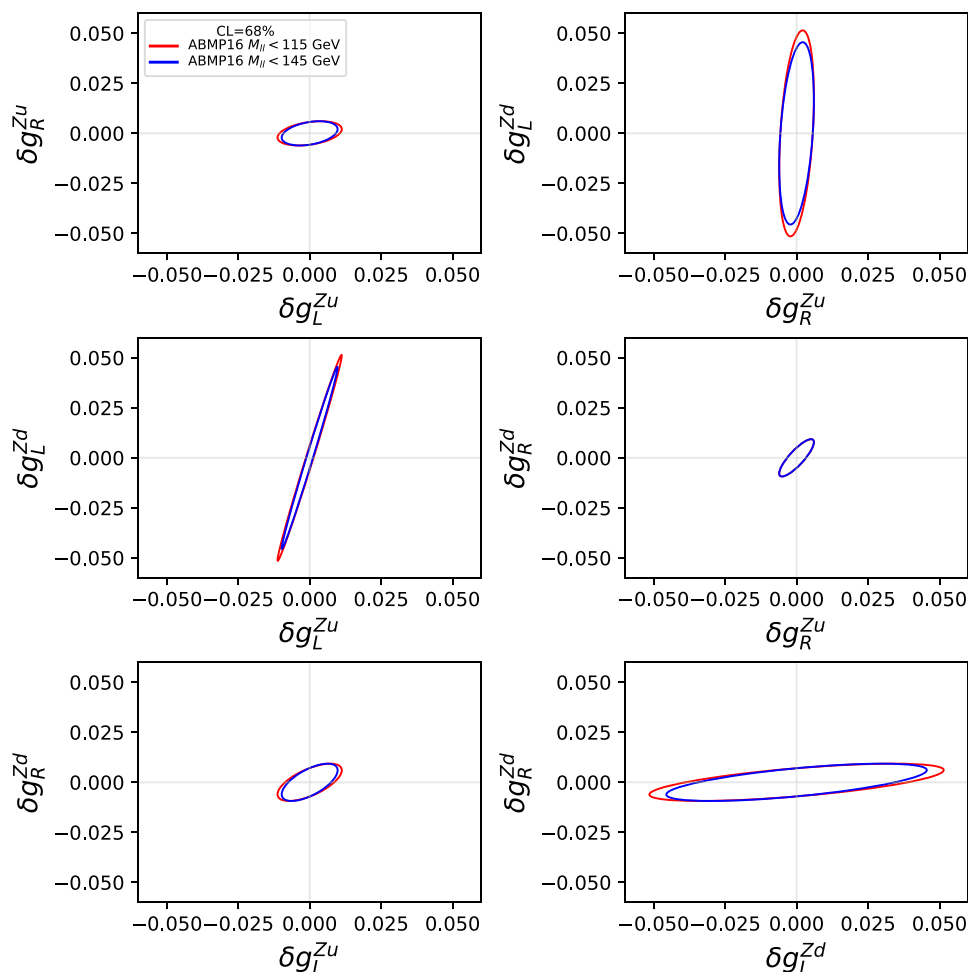


Fig. 21 The linear contributions of four-fermion operators $C_{lq}^{(1)}$ and C_{eu} and the contributions of the vertex corrections to couplings δg_L^{Zu} , δg_R^{Zd} , δg_L^{Zu} and δg_R^{Zd} to A_{FB} as a function of M_{ll} . The dotted vertical line shows the value of the cut $M < 145$ GeV used in our analysis

In order to study a possible dependence of our results on the upper boundary of $M_{\ell\ell}$, we repeated our analysis for the HL-LHC scenario using the ABMP16 PDF set with pseudo-data restricted to the region $M_{\ell\ell} < 115$ GeV only. The fitted couplings are shown in Fig. 22, where the nominal results obtained with $M_{\ell\ell} < 145$ GeV are shown as well. On average, the uncertainties on the couplings increase by 7% if the cut $M_{\ell\ell} < 115$ GeV is applied. We consider this as a robustness check of our results. We note that with future precise measurements of A_{FB} in a wide kinematic region extending to $M_{\ell\ell} > 150$ GeV it should be possible to provide constraints on both the SM couplings and the four-fermion SMEFT operators, and leave this for future studies.

⁸ For our sensitivity study even larger contributions from four-fermion operators at a percent level should not affect the main conclusions regarding the sensitivity to the SM couplings.

Fig. 22 Allowed regions for all pairs of corrections to the Z couplings to u - and d -type quarks obtained in the HL-LHC scenario with the ABMP16 PDF set using the $M_{ll} < 145$ GeV and $M_{ll} < 115$ GeV cuts



References

1. CMS Collaboration, Measurement of the weak mixing angle using the forward–backward asymmetry of Drell–Yan events in pp collisions at 8 TeV. *Eur. Phys. J. C* **78**, 701 (2018). <https://doi.org/10.1140/epjc/s10052-018-6148-7>. [arXiv:1806.00863](https://arxiv.org/abs/1806.00863)
2. CMS Collaboration, Measurement of the Drell–Yan forward–backward asymmetry at high dilepton masses in proton–proton collisions at $\sqrt{s} = 13$ TeV. *JHEP* **2022**, 063 (2022). [https://doi.org/10.1007/JHEP08\(2022\)063](https://doi.org/10.1007/JHEP08(2022)063). [arXiv:2202.12327](https://arxiv.org/abs/2202.12327)
3. ATLAS Collaboration, Measurement of the effective leptonic weak mixing angle using electron and muon pairs from Z -boson decay in the ATLAS experiment at $\sqrt{s} = 8$ TeV, ATLAS-CONF-2018-037 (2018)
4. ATLAS Collaboration, Prospect for a measurement of the Weak Mixing Angle in $pp \rightarrow Z/\gamma^* \rightarrow e^+e^-$ events with the ATLAS detector at the High Luminosity Large Hadron Collider, ATL-PHYS-PUB-2018-037 (2018)
5. ALEPH, DELPHI, L3, OPAL, SLD, LEP Electroweak Working Group, SLD Electroweak Group, SLD Heavy Flavour Group Collaboration, Precision electroweak measurements on the Z resonance. *Phys. Rep.* **427**, 257 (2006). <https://doi.org/10.1016/j.physrep.2005.12.006>. [arXiv:hep-ex/0509008](https://arxiv.org/abs/hep-ex/0509008)
6. CDF, D0 Collaboration, Tevatron Run II combination of the effective leptonic electroweak mixing angle. *Phys. Rev. D* **97**, 112007 (2018). <https://doi.org/10.1103/PhysRevD.97.112007>. [arXiv:1801.06283](https://arxiv.org/abs/1801.06283)
7. E. Accomando, J. Fiaschi, F. Hautmann, S. Moretti, Constraining parton distribution functions from neutral current Drell–Yan measurements. *Phys. Rev. D* **98**, 013003 (2018). <https://doi.org/10.1103/PhysRevD.98.013003>. [arXiv:1712.06318](https://arxiv.org/abs/1712.06318)
8. E. Accomando, J. Fiaschi, F. Hautmann, S. Moretti, Neutral current forward–backward asymmetry: from θ_W to PDF determinations. *Eur. Phys. J. C* **78**, 663 (2018). <https://doi.org/10.1140/epjc/s10052-018-6120-6>. [arXiv:1805.09239](https://arxiv.org/abs/1805.09239)
9. E. Accomando et al., PDF profiling using the forward–backward asymmetry in neutral current Drell–Yan production. *JHEP* **10**, 176 (2019). [https://doi.org/10.1007/JHEP10\(2019\)176](https://doi.org/10.1007/JHEP10(2019)176). [arXiv:1907.07727](https://arxiv.org/abs/1907.07727)
10. H. Abdolmaleki et al., Forward-backward Drell–Yan asymmetry and PDF determination, in *54th Rencontres de Moriond on QCD and High Energy Interactions, ARISF, 7* (2019), pp. 211–214. [arXiv:1907.08301](https://arxiv.org/abs/1907.08301)
11. J. Fiaschi et al., Lepton-charge and forward-backward asymmetries in Drell–Yan processes for precision electroweak measurements and new physics searches. *Nucl. Phys. B* **968**,

- 115444 (2021). <https://doi.org/10.1016/j.nuclphysb.2021.115444>. arXiv:2103.10224
12. T.-J. Hou et al., New CTEQ global analysis of quantum chromodynamics with high-precision data from the LHC. *Phys. Rev. D* **103**, 014013 (2021). <https://doi.org/10.1103/PhysRevD.103.014013>. arXiv:1912.10053
 13. S. Bailey, T. Cridge, L.A. Harland-Lang, A.D. Martin, R.S. Thorne, Parton distributions from LHC, HERA, Tevatron and fixed target data: MSHT20 PDFs. *Eur. Phys. J. C* **81**, 341 (2021). <https://doi.org/10.1140/epjc/s10052-021-09057-0>. arXiv:2012.04684
 14. NNPDF Collaboration, The path to proton structure at 1% accuracy. *Eur. Phys. J. C* **82**, 428 (2022). <https://doi.org/10.1140/epjc/s10052-022-10328-7>. arXiv:2109.02653
 15. S. Alekhin, J. Blümlein, S. Moch, R. Placakyte, Parton distribution functions, α_s , and heavy-quark masses for LHC Run II. *Phys. Rev. D* **96**, 014011 (2017). <https://doi.org/10.1103/PhysRevD.96.014011>. arXiv:1701.05838
 16. H1, ZEUS Collaboration, Combination of measurements of inclusive deep inelastic $e^\pm p$ scattering cross sections and QCD analysis of HERA data. *Eur. Phys. J. C* **75**, 580 (2015). <https://doi.org/10.1140/epjc/s10052-015-3710-4>. arXiv:1506.06042
 17. J. Fiaschi, F. Giuliani, F. Hautmann, S. Moch, S. Moretti, Z' -boson dilepton searches and the high- x quark density. *Phys. Lett. B* **841**, 137915 (2023). <https://doi.org/10.1016/j.physletb.2023.137915>. arXiv:2211.06188
 18. E. Accomando et al., Production of Z' -boson resonances with large width at the LHC. *Phys. Lett. B* **803**, 135293 (2020). <https://doi.org/10.1016/j.physletb.2020.135293>. arXiv:1910.13759
 19. J. Fiaschi et al., Enhancing the large hadron collider sensitivity to charged and neutral broad resonances of new gauge sectors. *JHEP* **02**, 179 (2022). [https://doi.org/10.1007/JHEP02\(2022\)179](https://doi.org/10.1007/JHEP02(2022)179). arXiv:2111.0969
 20. E. Accomando et al., The effect of real and virtual photons in the di-lepton channel at the LHC. *Phys. Lett. B* **770**, 1 (2017). <https://doi.org/10.1016/j.physletb.2017.04.025>. arXiv:1612.08168
 21. E. Accomando et al., Impact of the photon-initiated process on Z' -boson searches in di-lepton final states at the LHC, 9 (2016). arXiv:1609.07788
 22. E. Accomando et al., Photon-initiated production of a dilepton final state at the LHC: cross section versus forward–backward asymmetry studies. *Phys. Rev. D* **95**, 035014 (2017). <https://doi.org/10.1103/PhysRevD.95.035014>. arXiv:1606.06646
 23. A. Bodek, J. Han, A. Khukhunaishvili, W. Sakumoto, Using Drell–Yan forward–backward asymmetry to reduce PDF uncertainties in the measurement of electroweak parameters. *Eur. Phys. J. C* **76**, 115 (2016). <https://doi.org/10.1140/epjc/s10052-016-3958-3>. arXiv:1507.02470
 24. R.D. Ball, A. Candido, S. Forte, F. Hekhorn, E.R. Nocera, J. Rojo et al., Parton distributions and new physics searches: the Drell–Yan forward–backward asymmetry as a case study. *Eur. Phys. J. C* **82**, 1160 (2022). <https://doi.org/10.1140/epjc/s10052-022-11133-y>. arXiv:2209.08115
 25. Y. Fu, R. Brock, D. Hayden, C.-P. Yuan, Probing Parton distribution functions at large x via Drell–Yan forward–backward asymmetry. arXiv:2307.07839
 26. S. Yang, Y. Fu, M. Liu, L. Han, T.-J. Hou, C.P. Yuan, Factorization of the forward–backward asymmetry and measurements of the weak mixing angle and proton structure at hadron colliders. *Phys. Rev. D* **106**, 033001 (2022). <https://doi.org/10.1103/PhysRevD.106.033001>. arXiv:2202.13628
 27. S. Yang, M. Xie, Y. Fu, Z. Zhao, M. Liu, L. Han et al., Boost asymmetry of the diboson productions in pp collisions. *Phys. Rev. D* **106**, L051301 (2022). <https://doi.org/10.1103/PhysRevD.106.L051301>. arXiv:2207.02072
 28. M. Xie, S. Yang, Y. Fu, M. Liu, L. Han, T.-J. Hou et al., Measurement of the proton structure parameters in the forward–backward charge asymmetry. *Phys. Rev. D* **107**, 054008 (2023). <https://doi.org/10.1103/PhysRevD.107.054008>. arXiv:2209.13143
 29. S. Yang, Y. Fu, M. Liu, R. Zhang, T.-J. Hou, C. Wang et al., Reduction of the electroweak correlation in the PDF updating by using the forward–backward asymmetry of Drell–Yan process. *Eur. Phys. J. C* **82**, 368 (2022). <https://doi.org/10.1140/epjc/s10052-022-10280-6>. arXiv:2108.06550
 30. Y. Fu, S. Yang, M. Liu, L. Han, T.-J. Hou, C. Schmidt et al., Reduction of PDF uncertainty in the measurement of the weak mixing angle at the ATLAS experiment. *Chin. Phys. C* **45**, 053001 (2021). <https://doi.org/10.1088/1674-1137/abe36d>. arXiv:2008.03853
 31. C. Schmidt, J. Pumplin, C.P. Yuan, P. Yuan, Updating and optimizing error parton distribution function sets in the Hessian approach. *Phys. Rev. D* **98**, 094005 (2018). <https://doi.org/10.1103/PhysRevD.98.094005>. arXiv:1806.0795
 32. C. Willis, R. Brock, D. Hayden, T.-J. Hou, J. Isaacson, C. Schmidt et al., New method for reducing parton distribution function uncertainties in the high-mass Drell–Yan spectrum. *Phys. Rev. D* **99**, 054004 (2019). <https://doi.org/10.1103/PhysRevD.99.054004>. arXiv:1809.09481
 33. W. Buchmuller, D. Wyler, Effective Lagrangian analysis of new interactions and flavor conservation. *Nucl. Phys. B* **268**, 621 (1986). [https://doi.org/10.1016/0550-3213\(86\)90262-2](https://doi.org/10.1016/0550-3213(86)90262-2)
 34. G. Isidori, F. Wilsch, D. Wyler, The Standard Model effective field theory at work. arXiv:2303.16922
 35. I. Brivio, M. Trott, The Standard Model as an effective field theory. *Phys. Rep.* **793**, 1 (2019). <https://doi.org/10.1016/j.physrep.2018.11.002>. arXiv:1706.08945
 36. SMEFT Collaboration, Combined SMEFT interpretation of Higgs, diboson, and top quark data from the LHC. *JHEP* **11**, 089 (2021). [https://doi.org/10.1007/JHEP11\(2021\)089](https://doi.org/10.1007/JHEP11(2021)089). arXiv:2105.00006
 37. J. Ellis, M. Madigan, K. Mimasu, V. Sanz, T. You, Top, Higgs, diboson and electroweak fit to the Standard Model effective field theory. *JHEP* **04**, 279 (2021). [https://doi.org/10.1007/JHEP04\(2021\)279](https://doi.org/10.1007/JHEP04(2021)279). arXiv:2012.02779
 38. I. Brivio, Y. Jiang, M. Trott, The SMEFTsim package, theory and tools. *JHEP* **12**, 070 (2017). [https://doi.org/10.1007/JHEP12\(2017\)070](https://doi.org/10.1007/JHEP12(2017)070). arXiv:1709.06492
 39. L. Bellafronte, S. Dawson, P.P. Giardino, The importance of flavor in SMEFT electroweak precision fits. *JHEP* **05**, 208 (2023). [https://doi.org/10.1007/JHEP05\(2023\)208](https://doi.org/10.1007/JHEP05(2023)208). arXiv:2304.00029
 40. S. Dawson, P.P. Giardino, A. Ismail, Standard model EFT and the Drell–Yan process at high energy. *Phys. Rev. D* **99**, 035044 (2019). <https://doi.org/10.1103/PhysRevD.99.035044>. arXiv:1811.12260
 41. R. Boughezal, Y. Huang, F. Petriello, Impact of high invariant-mass Drell–Yan forward–backward asymmetry measurements on SMEFT fits. *Phys. Rev. D* **108**, 076008 (2023). <https://doi.org/10.1103/PhysRevD.108.076008>. arXiv:2303.08257
 42. R. Boughezal, E. Mereghetti, F. Petriello, Dilepton production in the SMEFT at $\mathcal{O}(1/\Lambda^4)$. *Phys. Rev. D* **104**, 095022 (2021). <https://doi.org/10.1103/PhysRevD.104.095022>. arXiv:2106.05337
 43. V. Bresó-Pla, A. Falkowski, M. González-Alonso, A_{FB} in the SMEFT: precision Z physics at the LHC. *JHEP* **08**, 021 (2021). [https://doi.org/10.1007/JHEP08\(2021\)021](https://doi.org/10.1007/JHEP08(2021)021). arXiv:2103.12074
 44. L. Allwicher, D.A. Faroughy, F. Jaffredo, O. Sumensari, F. Wilsch, Drell–Yan tails beyond the Standard Model. *JHEP* **03**, 064 (2023). [https://doi.org/10.1007/JHEP03\(2023\)064](https://doi.org/10.1007/JHEP03(2023)064). arXiv:2207.10714
 45. A. Greljo, S. Iranipour, Z. Kassabov, M. Madigan, J. Moore, J. Rojo et al., Parton distributions in the SMEFT from high-energy Drell–Yan tails. *JHEP* **07**, 122 (2021). [https://doi.org/10.1007/JHEP07\(2021\)122](https://doi.org/10.1007/JHEP07(2021)122). arXiv:2104.02723
 46. E. Hammou, Z. Kassabov, M. Madigan, M.L. Mangano, L. Mantani, J. Moore et al., Hide and seek: how PDFs can conceal new physics. *JHEP* **11**, 090 (2023). [https://doi.org/10.1007/JHEP11\(2023\)090](https://doi.org/10.1007/JHEP11(2023)090). arXiv:2307.10370

47. B. Grzadkowski, M. Iskrzynski, M. Misiak, J. Rosiek, Dimension-Six Terms in the Standard Model Lagrangian. *JHEP* **10**, 085 (2010). [https://doi.org/10.1007/JHEP10\(2010\)085](https://doi.org/10.1007/JHEP10(2010)085). arXiv:1008.4884
48. S. Alekhin et al., HERAFitter. *Eur. Phys. J. C* **75**, 304 (2015). <https://doi.org/10.1140/epjc/s10052-015-3480-z>. arXiv:1410.4412
49. xFitter Collaboration, xFitter: An Open Source QCD analysis framework. A resource and reference document for the Snowmass study, 6 (2022). arXiv:2206.12465
50. xFitter code repository and documentation (public access) <https://gitlab.cern.ch/fitters/xfitter>. Accessed 24 Aug 2023
51. F. Gianotti et al., Physics potential and experimental challenges of the LHC luminosity upgrade. *Eur. Phys. J. C* **39**, 293 (2005). <https://doi.org/10.1140/epjc/s2004-02061-6>. arXiv:hep-ph/0204087
52. P. Azzi et al., Report from Working Group 1: Standard Model Physics at the HL-LHC and HE-LHC. CERN Yellow Rep. Monogr. **7**, 1 (2019). <https://doi.org/10.23731/CYRM-2019-007.1>. arXiv:1902.04070
53. X. Cid Vidal et al., Report from Working Group 3: Beyond the Standard Model physics at the HL-LHC and HE-LHC. CERN Yellow Rep. Monogr. **7**, 585 (2019). <https://doi.org/10.23731/CYRM-2019-007.585>. arXiv:1812.07831
54. J.C. Collins, D.E. Soper, Angular Distribution of Dileptons in High-Energy Hadron Collisions. *Phys. Rev. D* **16**, 2219 (1977). <https://doi.org/10.1103/PhysRevD.16.2219>
55. S. Dittmaier, M. Huber, Radiative corrections to the neutral-current Drell-Yan process in the Standard Model and its minimal supersymmetric extension. *JHEP* **01**, 060 (2010). [https://doi.org/10.1007/JHEP01\(2010\)060](https://doi.org/10.1007/JHEP01(2010)060). arXiv:0911.2329
56. C.M.S. Collaboration, Search for physics beyond the standard model in dilepton mass spectra in proton-proton collisions at $\sqrt{s} = 8$ TeV. *JHEP* **04**, 025 (2015). [https://doi.org/10.1007/JHEP04\(2015\)025](https://doi.org/10.1007/JHEP04(2015)025). arXiv:1412.6302
57. S. Alekhin, A. Kardos, S. Moch, Z. Trócsányi, Precision studies for Drell-Yan processes at NNLO. *Eur. Phys. J. C* **81**, 573 (2021). <https://doi.org/10.1140/epjc/s10052-021-09361-9>. arXiv:2104.02400
58. J. Alwall, R. Frederix, S. Frixione, V. Hirschi, F. Maltoni, O. Mattelaer et al., The automated computation of tree-level and next-to-leading order differential cross sections, and their matching to parton shower simulations. *JHEP* **07**, 079 (2014). [https://doi.org/10.1007/JHEP07\(2014\)079](https://doi.org/10.1007/JHEP07(2014)079). arXiv:1405.0301
59. T. Carli, D. Clements, A. Cooper-Sarkar, C. Gwenlan, G.P. Salam, F. Siegert et al., A posteriori inclusion of parton density functions in NLO QCD final-state calculations at hadron colliders: The APPLGRID Project. *Eur. Phys. J. C* **66**, 503 (2010). <https://doi.org/10.1140/epjc/s10052-010-1255-0>. arXiv:0911.2985
60. V. Bertone, R. Frederix, S. Frixione, J. Rojo, M. Sutton, aMCfast: automation of fast NLO computations for PDF fits. *JHEP* **08**, 166 (2014). [https://doi.org/10.1007/JHEP08\(2014\)166](https://doi.org/10.1007/JHEP08(2014)166). arXiv:1406.7693
61. ATLAS Collaboration, Studies of the muon momentum calibration and performance of the ATLAS detector with pp collisions at $\sqrt{s} = 13$ TeV. *Eur. Phys. J. C* **83**, 686 (2023). <https://doi.org/10.1140/epjc/s10052-023-11584-x>. arXiv:2212.07338
62. ATLAS Collaboration, Electron and photon energy calibration with the ATLAS detector using 2015–2016 LHC proton–proton collision data. *JINST* **14**, P03017 (2019). <https://doi.org/10.1088/1748-0221/14/03/P03017>. arXiv:1812.03848
63. F. James, M. Roos, Minuit: A System for Function Minimization and Analysis of the Parameter Errors and Correlations. *Comput. Phys. Commun.* **10**, 343 (1975). [https://doi.org/10.1016/0010-4655\(75\)90039-9](https://doi.org/10.1016/0010-4655(75)90039-9)
64. H. Paukkunen, P. Zurita, PDF reweighting in the Hessian matrix approach. *JHEP* **12**, 100 (2014). [https://doi.org/10.1007/JHEP12\(2014\)100](https://doi.org/10.1007/JHEP12(2014)100). arXiv:1402.6623
65. HERAFitter Developers' Team Collaboration, QCD analysis of W - and Z -boson production at Tevatron. *Eur. Phys. J. C* **75**, 458 (2015). <https://doi.org/10.1140/epjc/s10052-015-3655-7>. arXiv:1503.05221
66. S. Alekhin, M.V. Garzelli, S. Kulagin, S.O. Moch, Impact of SeaQuest data on PDF fits at large x . *Eur. Phys. J. C* **83**, 829 (2023). <https://doi.org/10.1140/epjc/s10052-023-11999-6>. arXiv:2306.01918
67. H1 Collaboration, Determination of electroweak parameters in polarised deep-inelastic scattering at HERA. *Eur. Phys. J. C* **78**, 777 (2018). <https://doi.org/10.1140/epjc/s10052-018-6236-8>. arXiv:1806.01176
68. D0 Collaboration, Measurement of $\sin^2 \theta_{\text{eff}}^{\ell}$ and Z -light quark couplings using the forward-backward charge asymmetry in $p\bar{p} \rightarrow Z/\gamma^* \rightarrow e^+e^-$ events with $\mathcal{L} = 5.0 \text{ fb}^{-1}$ at $\sqrt{s} = 1.96$ TeV. *Phys. Rev. D* **84**, 012007 (2011). <https://doi.org/10.1103/PhysRevD.84.012007>. arXiv:1104.4590
69. D. Britzger, M. Klein, H. Spiesberger, Electroweak physics in inclusive deep inelastic scattering at the LHeC. *Eur. Phys. J. C* **80**, 831 (2020). <https://doi.org/10.1140/epjc/s10052-020-8367-y>. arXiv:2007.11799
70. D. Britzger, M. Klein and H. Spiesberger, Precision electroweak measurements at the LHeC and the FCC-eh. *PoS EPS-HEP2021*, 485 (2022). <https://doi.org/10.22323/1.398.0485>. arXiv:2203.06237
71. ZEUS Collaboration, Combined QCD and electroweak analysis of HERA data. *Phys. Rev. D* **93**, 092002 (2016). <https://doi.org/10.1103/PhysRevD.93.092002>. arXiv:1603.09628
72. I. Abt, A.M. Cooper-Sarkar, B. Foster, C. Gwenlan, V. Myronenko, O. Turkot et al., Combined Electroweak and QCD Fit to HERA Data. *Phys. Rev. D* **94**, 052007 (2016). <https://doi.org/10.1103/PhysRevD.94.052007>. arXiv:1604.05083
73. LHeC, FCC-he Study Group Collaboration, The large hadron–electron collider at the HL-LHC. *J. Phys. G* **48**, 110501 (2021). <https://doi.org/10.1088/1361-6471/abf3ba>. arXiv:2007.14491
74. FCC Collaboration, FCC physics opportunities: future circular collider conceptual design report volume 1. *Eur. Phys. J. C* **79**, 474. <https://doi.org/10.1140/epjc/s10052-019-6904-3>